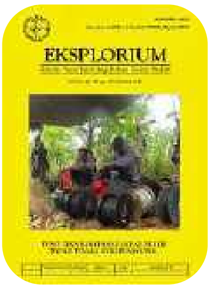

# EKSPLORIUM : BULETIN PUSAT PENGEMBANGAN BAHAN GALIAN NUKLIR

BADAN TENAGA NUKLIR NASIONAL

P-ISSN : 08541418 E-ISSN : 2503426x Subject Area : Science

0
Impact

491
Google Citations

Sinta 2
Current Acreditation

Google Scholar Garuda Website Editor URL

History Accreditation

2018 2019 2020 2021 2022 2023 2024 2025

**Garuda** Google Scholar

Search...

Ore Mineralization Characteristics in Hydrothermal Alteration at Mangunharjo and Surrounding Areas, Pacitan, Indonesia
Badan Riset dan Inovasi Nasional EKSPLORIUM Vol 43, No 1 (2022): Mei 2022 13-22
2022 DOI: 10.17146/eksplorium.2022.43.1.6194 Accred : Sinta 2

Sub-surface Geological Modeling Based on Gravity Residual Data in Adang Volcanic Rock Area, Mamuju, West Sulawesi Province
Badan Riset dan Inovasi Nasional EKSPLORIUM Vol 43, No 1 (2022): Mei 2022 23-28
2022 DOI: 10.17146/eksplorium.2022.43.1.6089 Accred : Sinta 2

Tectonic Pattern Imaging of Southern Sumatra Region Using Double Difference Seismic Tomography
Badan Riset dan Inovasi Nasional EKSPLORIUM Vol 43, No 1 (2022): Mei 2022 29-40
2022 DOI: 10.17146/eksplorium.2022.43.1.6603 Accred : Sinta 2

Geostatistical Ore Body Modeling on Uranium Mineralization in Remaja Sector, Kalan Area, West Kalimantan
Badan Riset dan Inovasi Nasional EKSPLORIUM Vol 43, No 1 (2022): Mei 2022 41-58
2022 DOI: 10.17146/eksplorium.2022.43.1.6622 Accred : Sinta 2

Review on Granitic Rocks in Sumatra: Intrusion Process, Classification, Mineralization and Potential Uses

Badan Riset dan Inovasi Nasional EKSPLORIUM Vol 43, No 1 (2022): Mei 2022 1-12

2022 DOI: 10.17146/eksplorium.2022.43.1.6471 Accred : Sinta 2

Cover and Table of Content

Badan Riset dan Inovasi Nasional EKSPLORIUM Vol 43, No 1 (2022): Mei 2022 i-vii

2022 DOI: - Accred : Sinta 2

Peningkatan Perolehan Uranium, Torium, dan Logam Tanah Jarang dalam Residu Pelarutan Parsial pada Pengolahan Monasit

Pusat Teknologi Bahan Galian Nuklir - BATAN EKSPLORIUM Vol 42, No 2 (2021): November 2021 141-148

2021 DOI: 10.17146/eksplorium.2021.42.2.6044 Accred : Sinta 2

Indikasi Sesar Naik di Plampang, Pulau Sumbawa Berdasarkan Analisis Gempa Bumi 13 Juni 2020

Pusat Teknologi Bahan Galian Nuklir - BATAN EKSPLORIUM Vol 42, No 2 (2021): November 2021 111-118

2021 DOI: 10.17146/eksplorium.2021.42.2.6273 Accred : Sinta 2

Distribution and Mineralogical Characteristic of Raya Volcanics, West Kalimantan

Pusat Teknologi Bahan Galian Nuklir - BATAN EKSPLORIUM Vol 42, No 2 (2021): November 2021 77-90

2021 DOI: 10.17146/eksplorium.2021.42.2.6511 Accred : Sinta 2

Penentuan Komposisi Bahan Bakar Nabati Dalam Bahan Bakar Minyak Campuran Menggunakan Metode Direct Counting C-14

Pusat Teknologi Bahan Galian Nuklir - BATAN EKSPLORIUM Vol 42, No 2 (2021): November 2021 149-162

2021 DOI: 10.17146/eksplorium.2021.42.2.6363 Accred : Sinta 2

Previous 1 2 3 4 5 Next

Page 1 of 18 | Total Records 176

p-ISSN 0854-1418
e-ISSN 2503-426X

Accreditation by the Directorate General of Higher Education,
Research and Technology No. 158/E/KPT/2021

# EKSPLORIUM

## Buletin Pusat Pengembangan Bahan Galian Nuklir
## *Bulletin of the Center for Nuclear Minerals Development*

Volume 45 No. 1, May 2024

DIRECTORATE OF REPOSITORIES, MULTIMEDIA, AND SCIENTIFIC PUBLICATION
NATIONAL RESEARCH AND INNOVATION AGENCY

| | | | | | | |
|---|---|---|---|---|---|---|
| EKSPLORIUM | Volume<br>45 | No.<br>1 | Pages<br>1-56 | Jakarta<br>May 2024 | *p*-ISSN 0854- 1418<br>*e*-ISSN 2503-426X | Accreditation No.<br>158/E/KPT/2021 |

**p-ISSN 0854-1418**
**e-ISSN 2503-426X**
**Accreditation by the Directorate General of Higher Education,**
**Research and Technology No. 158/E/KPT/2021**

# EKSPLORIUM

## Buletin Pusat Pengembangan Bahan Galian Nuklir

*Bulletin of the Center for Nuclear Minerals Development*

**Volume 45 No. 1, May 2024**

**Eksplorium**, the Bulletin of the Center for Nuclear Minerals Development, is a scientific journal which contains the results of studies, research, and development of nuclear geology with the scope of geology, exploration, mining, processing of nuclear minerals, and environmental safety as well as the development of nuclear technology for people's welfare. **Eksplorium** published 2 (two) times a year, in May and November.

**Chief Editor**
Dr. Ir. I Gde Sukadana, M.Eng., IPM, BRIN, Indonesia

**Associate Editors**
Frederikus Dian Indrastomo, M.T., BRIN, Indonesia
Heri Syaeful, M.T., BRIN, Indonesia
Kurnia Setiawan Widana, M.T., BRIN, Indonesia
Roni Cahya Ciputra, M.T., BRIN, Indonesia

**Editorial Board**
Prof. Dr. Muhayatun Santoso, M.T., BRIN, Indonesia
Prof. Dr. Ir. Ildrem Syafri, DEA., Padjajaran University, Indonesia
Prof. Dr. Eng. Sidik Permana, M.Eng., Institut Teknologi Bandung, Indonesia
Prof. Himawan Bayumurti Petrus, M.E., D.Eng., Universitas Gadjah Mada, Indonesia
Dr.rer.nat. Ir. I Wayan Warmada, IPM, Universitas Gadjah Mada, Indonesia
Dr. Sri Mulyaningsih, Institut Sains dan Teknologi "AKPRIND" Yogyakarta, Indonesia
Dr. Hill Gendoet Hartono, Institut Teknologi Nasional Yogyakarta, Indonesia
Dr. Sulaksana Permana, M.T., Gunadarma University, Indonesia
Iwan Susanto, Ph.D., Politeknik Negeri Jakarta, Indonesia
Rahman Yaccub, M.Sc. Ph.D., Malaysia Nuclear Agency, Malaysia
Pipat Laowattanabandit, M.Sc., Ph.D., Chulalongkorn University, Thailand
Abduelhamed Mohamed Salem Ethman, M.Sc., Libyan Atomic Energy Establishment, Libya
Ir. Yarianto Sugeng Budi Susilo, M.Si., BRIN, Indonesia
Yuniarti Ulfa, M.Sc., Politeknik Geologi dan Pertambangan "AGP", Indonesia

**Copy Editor**
Windi Anarta Draniswari, M.T., BRIN, Indonesia
Ersina Rakhma, M.T., BRIN, Indonesia
Tyto Baskara Adimedha, M.Eng., BRIN, Indonesia
Apriwi Zulfitri, M.Sc., BRIN, Indonesia

**Layout Editor**
M. Ilham Bayquni, M.T., BRIN, Indonesia
Mirna Berliana Garwan, S.T., BRIN, Indonesia

**Managing Editor**
Dra. Noeraida, BRIN, Indonesia
Andri Agus Rahman, A.Md., BRIN, Indonesia

Photo caption: The fault-controlled Handeuleum Hotspring of Mount Endut Geothermal Area, West Java (Contributor: Mochamad Ikral Pamungkas)

**Publisher:**
**DIRECTORATE OF REPOSITORIES, MULTIMEDIA, AND SCIENTIFIC PUBLICATION**
**NATIONAL RESEARCH AND INNOVATION AGENCY**

Editorial Address:
Building 720, B.J. Habibie Science and Technology Area, South Tangerang, Banten 15314
Telp. 081 110 646 830, E-mail: eksplorium@brin.go.id
**Website: http://jurnal.batan.go.id/index.php/eksplorium**

*p*-ISSN 0854-1418
*e*-ISSN 2503-426X

**EKSPLORIUM**
Buletin Pusat Pengembangan Bahan Galian Nuklir
*Bulletin of the Center for Nuclear Minerals Development*
Volume 45, No. 1, May 2024

# FOREWORD

Dear Readers,

This edition of **Eksplorium** contains five (5) research articles from various fields. The first paper describes uranium and Rare Earth Element (REE) characterization from Rirang uranium Deposits with titled “Distribution and Characteristics of Rare Earth Elements in Uranium-Ore Deposits from Rirang Area, West Kalimantan Province, Indonesia” The second paper is about identification of radioactive and REE in placer deposits with titled “Characterization of Radioactive and Rare Earth Elements in Heavy Minerals from River Sediments in Marau Region, Ketapang, West Kalimantan”. The third paper discusses about development method for geological structure identification titled “Geological Structure Identification Using GGMplus Satellite Gravity Data in The Area Surrounding Mount Tampomas”. The fourth paper is a study for land suitability analysis, with titled “Geology and Land Suitability Analysis for Final Processing Waste Site in Ambon Island”. The last paper is about the method validation for the determination of REE oxide with titled “Validation of The Gravimetry Method for Determining Rare Earth Elements Oxides”

We believe that **Eksplorium** can benefit readers, especially in developing insights into nuclear minerals technology, including geology, mining, processing, and the environment.

Editor in Chief

*p*-ISSN 0854-1418
*e*-ISSN 2503-426X

**EKSPLORIUM**
Buletin Pusat Pengembangan Bahan Galian Nuklir
*Bulletin of the Center for Nuclear Minerals Development*
Volume 45, No. 1, May 2024

## Table of Contents

*p*-ISSN 0854-1418
*e*-ISSN 2503-426X

**EKSPLORIUM**
Buletin Pusat Pengembangan Bahan Galian Nuklir
*Bulletin of the Center for Nuclear Minerals Development*
Volume 45, No. 1, May 2024

# Distribution and Characteristics of Rare Earth Elements in Uranium-Ore Deposits from Rirang Area, West Kalimantan Province, Indonesia

**Tyto Baskara Adimedha[1*], Rayhan Aldizan Farrenzo[2], I Gde Sukadana[1], Rosmalia Dita Nugraheni[2], Fadiah Pratiwi[1], Roni Cahya Ciputra[1], Frederikus Dian Indrastomo[1], Heri Syaeful[1], Yoshi Rachael[1]**

[1]Research Center for Nuclear Material and Radioactive Waste Technology, ORTN-BRIN
KST B. J. Habibie, South Tangerang, Banten, 15314, Indonesia
[2]Department of Geological Engineering, Faculty of Earth Technology and Energy, Universitas Trisakti
Letjen S. Parman St., No.1, Campus A, West Jakarta, DKI Jakarta, 11440, Indonesia
*E-mail: tyto001@brin.go.id

Article received: 15 May 2024, revised: 30 May 2024, accepted: 31 May 2024
DOI: 10.55981/eksplorium.2024.7058

## ABSTRACT

Uranium and rare earth elements (REE) are essential elements for the development of green environmentally friendly, and sustainable energy. To meet the increasing demand for these raw materials, Indonesia has taken steps to explore and map potential deposits, including the Rirang Sector in Melawi Regency, West Kalimantan. However, the available information on the mineralization of these elements in the area is limited. Therefore, this study aimed to provide a detailed characterization on the petrology and geochemical characteristics of uranium ore and to synthesize the mineral genesis of uranium and REE-bearing ore in the Rirang Sector. The analytical methods used included petrography, micro-XRF, and geochemical analysis. The results showed that uranium mineralization was present in brannerites, uranophane, and swamboite associated with tourmaline and monazite ore. Similarly, REE concentrations were hosted by REE-bearing minerals, such as monazite, xenotime, and loparite. Geochemically, the uranium concentration in the monazite ore ranged from 1,110–28,440 ppm, while the total REE (TREE) concentration varied between 85,320 to 138,488 ppm. The formation of uranium and REE mineralization were due to the metasomatism process and its association with the Na-rich fluid of felsic intrusion. Notably, the weathering process did not enrich uranium and REE content in the soil but rather decreased it due to the leaching process and the absence of clay minerals capable of absorbing the REE cations on the surface of clay crystal structures.

**Keywords:** West Kalimantan, monazite, rare earth elements, tourmaline, uranium

*p*-ISSN 0854-1418
*e*-ISSN 2503-426X

**EKSPLORIUM**
Buletin Pusat Pengembangan Bahan Galian Nuklir
*Bulletin of the Center for Nuclear Minerals Development*
Volume 45, No. 1, May 2024

# Characterization of Radioactive and Rare Earth Elements in Heavy Minerals from River Sediments in Marau Region, Ketapang, West Kalimantan

**Fadiah Pratiwi[1]*, Yoshi Rachael[1], Widodo[2], Rachman Fauzi[3], Nunik Madyaningarum[4], Tyto Baskara Adimedha[1], Frederikus Dian Indrastomo[1], I Gde Sukadana[1]**

[1]Research Center for Nuclear Material and Radioactive Waste Technology, ORTN-BRIN
KST B. J. Habibie, South Tangerang, Banten, 15314, Indonesia
[2]Polytechnic Institutes of Nuclear Technology
Babarsari St., PO BOX 6101/YKKB, Sleman, D. I. Yogyakarta, 55281, Indonesia
[3]Research Center for Geological Resources, ORKM-BRIN
KST Samaun Samadikun, Bandung, 40135, Indonesia
[4]Research Center for Safety, Metrology, and Nuclear Quality Technology, ORTN-BRIN
KST B. J. Habibie, South Tangerang, Banten, 15314, Indonesia
*E-mail: fadi005@brin.go.id

Article received: 7 December 2023, revised: 29 May 2024, accepted: 31 May 2024
DOI: 10.55981/eksplorium.2024.6971

## ABSTRACT

Alluvium deposits from the Kendawangan River located in Marau, Ketapang, West Kalimantan have been known for their radioactive and rare earth mineral potential. In this paper, heavy minerals taken from alluvium deposits will be characterized to determine the elemental distribution of uranium, thorium, and rare earth elements in each mineral and their mineralogical composition. The samples are taken by panning and prepared using the flotation method to obtain heavy mineral concentrates. Geochemical analysis was carried out using a Bruker M4 Tornado plus Micro-XRF and continued with mineralogical analysis using AMICS (Advanced Mineral Identification and Characterization System) software. It was found that the distribution of heavy minerals from the sand samples was dominated by manganoan ilmenite, ilmenite, rutile, zircon, magnetite, and monazite, as well as thorite, cassiterite, xenotime, allanite, and other minerals in small quantities. Uranium, thorium, and rare earth elements are found in monazite, thorite, xenotime, zircon, and allanite.

**Keywords**: heavy minerals, Micro-XRF, radioactive minerals, rare earth element

*p*-ISSN 0854-1418
*e*-ISSN 2503-426X

**EKSPLORIUM**
Buletin Pusat Pengembangan Bahan Galian Nuklir
*Bulletin of the Center for Nuclear Minerals Development*
Volume 45, No. 1, May 2024

# Geological Structure Identification Using GGMplus Satellite Gravity Data in The Area Surrounding Mount Tampomas

**Haidar Prida Mazzaluna[1], Rustadi[1], Rahmat Catur Wibowo[1]***
[1]Department of Geophysical Engineering, Faculty of Engineering, Lampung University,
Sumantri Brojonegoro St. No.1, Bandar Lampung, Lampung, 35145, Indonesia
*E-mail: rahmat.caturwibowo@eng.unila.ac.id

Article received: 2 October 2023, revised: 2 April 2024, accepted: 22 April 2024
DOI: 10.55981/eksplorium.2024.6924

## ABSTRACT

Satellite gravity provides a new alternative in geological exploration with several advantages, such as low operational cost and large covering area. GGMplus satellite gravity data provide better accuracy for several applications such as lithology or fault identification. Satellite gravity provides a new alternative in geological exploration with several advantages, such as lower costs, broader area coverage, and easily accessible data. Mount Tampomas is one of the areas that has geothermal prospects and a mountain area that has many types of rock formations and faults. This research has been conducted using GGMplus satellite gravity data in the Mount Tampomas area to obtain the second vertical derivative (SVD) and identify the fault distribution in the area. The GGMplus Gravity Acceleration data was corrected and filtered to obtain SVD structures in the area. The structure in this area is dominantly trending northwest-southeast and west-east. The area around Mount Tampomas forms a structure in the form of a caldera. In addition, there are also structures trending north-south at coordinates 81500-82000 E. Some of these structures were overlaid with a geological map to see the suitability of the processed data with the geological conditions that have been studied. The comparison is done by overlaying the structure of the interpretation results and the contour of the value 0 from the Second Vertical Derivative (SVD) data so that we get four fault structures that correlate with the geological map, three calderas, and one lineament that correlates with the lineament map.

**Keywords:** Mount Tampomas, GGMplus, gravity method, geological structure.

*p*-ISSN 0854-1418
*e*-ISSN 2503-426X

**EKSPLORIUM**
Buletin Pusat Pengembangan Bahan Galian Nuklir
*Bulletin of the Center for Nuclear Minerals Development*
Volume 45, No. 1, May 2024

# Geology and Land Suitability Analysis for Final Processing Waste Site in Ambon Island

**Winardcova Vania Cerwyn Mailoa[1]*, Micky Kololu[1], Yuniarti Ulfa[2], Deni Juanda Puradimadja[3]**
[1]Program Study of Geological Engineering, Faculty of Engineering, Pattimura University,
Ir. M. Putuhena St., Kampus Poka, Kota Ambon, Maluku, 97223, Indonesia
[2]Program Study of Geological Engineering, Polytechnic of Geology and Mining "AGP"
Lodaya St., No. 38, Bandung, 40264, Indonesia
[3]Program Study of Geological Engineering, Faculty of Earth Science and Technology,
Institut Teknologi Bandung, Ganesha St., No.10, Bandung, West Java, 40132, Indonesia
*E-mail: mailovania@gmail.com

Article received: 18 March 2024, revised: 22 April 2024, accepted: 29 May 2024
DOI: 10.55981/eksplorium.2024.7042

## ABSTRACT

The production of waste in Ambon City increased from 200 tons per day to 297 tons per day between 2017 and 2021, yet the state of the Toisapu landfill in Ambon did not keep up with this growth. The Toisapu landfill has been in operation since 2007, however, due to its proximity to residential areas and slope of more than 20 percent, it is currently in an overload state and requires a re-evaluation. The goal of this study is to identify a different landfill to replace the Toisapu landfill that fulfills the Indonesian National Standards and functions as a Waste Processing and Final Processing Site (TPPAS). This study combines an evaluation of the geological and non-geological parameters using an environmental geological technique called Spatial Multi-Criteria Evaluation (SMCE). In order to determine the most possible land, the study findings for each parameter are superimposed, assigned a value, and then added together. According to the research's findings, Wakal, which has 126,668 hectares of land is the best option. Since the groundwater in this area is quite deep (>80 meters) and has low permeability, there is minimal possibility of leachate seepage contaminating the groundwater. Wakal, unlike the Toisapu landfill, is located far from inhabited areas and protected forests, with a slope of less than 20%.

**Keywords:** Ambon Island, waste, environmental geology, SMCE, waste processing, final processing.

*p*-ISSN 0854-1418
*e*-ISSN 2503-426X

**EKSPLORIUM**
Buletin Pusat Pengembangan Bahan Galian Nuklir
*Bulletin of the Center for Nuclear Minerals Development*
Volume 45, No. 1, May 2024

# Validation of The Gravimetry Method for Determining Rare Earth Elements Oxides

**Afiq Azfar Pratama[1]*, Amalia Ekaputri Hidayat[1], Rommy[1], Suci Indryati[1], Roza Indra Laksmana[1], Kurnia Trinopiawan[1], Tri Purwanti[1], Kurnia Setiawan Widana[1], Aditya Widian Putra[1], Mutia Anggraini[2], Dzaki Hasan Nasrullah[3]**
[1]Research Center for Nuclear Material and Radioactive Waste Technology, ORTN-BRIN
KST B. J. Habibie, South Tangerang, Banten, 15314, Indonesia
[2]Directorate of Laboratory Management Research Facilities and Science and Technology Park, DIRI-BRIN
KST B. J. Habibie, Serpong, South Tangerang, Banten 15314, Indonesia
[3]SMK-SMAK Bogor, Binamarga 1 St., Bogor, West Java, 16143, Indonesia
*E-mail: afiq001@gmail.com

Article received: 22 March 2024, revised: 2 May 2024, accepted: 29 May 2024
DOI: 10.55981/eksplorium.2024.6972

## ABSTRACT

The demand for minerals to meet technological developments is increasing, including minerals that contain rare earth elements (REE). The levels of REE in solids can be determined using conventional analysis methods (gravimetry) and instruments. Even though the instrument method provides more accurate results with a small amount of analyte, the cost is higher compared to the gravimetric method, which requires more analyte and provides good results. Therefore, the gravimetric method is a solution for areas with limited instruments and budgets. The study aims to validate the gravimetric method for determining REE oxides levels, evaluate its precision and accuracy, and assess its feasibility of use. In this study, two methods were used for REE analysis: the ASTM E2941-14 method with sample weight modification and the addition of acid to increase REE oxides recovery and a precipitation method using oxalic acid. The validation stages include sample dissolution, precipitation, filtration, and ash-making. The research results show that the RSD value is 0.3154, which is smaller than 2/3 of Horwitz's CV, namely 4.1727, which means it meets the precision acceptance requirements of ISO/IEC 17025:2017. The REE oxides recovery value, which indicates accuracy, also increased to 97.74%. Therefore, the gravimetric method can be used as an alternative for determining REE oxides levels.

**Keywords:** gravimetric methods, method validation, oxalic acid, REE oxides

*Eksplorium*
Volume 45 No. 1, Mei/November 2024: 1–16

*p*-ISSN 0854-1418
*e*-ISSN 2503-426X

# Distribution and Characteristics of Rare Earth Elements in Uranium-Ore Deposits from Rirang Area, West Kalimantan Province, Indonesia

**Tyto Baskara Adimedha[1*], Rayhan Aldizan Farrenzo[2], I Gde Sukadana[1], Rosmalia Dita Nugraheni[2], Fadiah Pratiwi[1], Roni Cahya Ciputra[1], Frederikus Dian Indrastomo[1], Heri Syaeful[1], Yoshi Rachael[1]**

[1]Research Center for Nuclear Mineral and Radioactive Waste Technology, The National Research and Innovation Agency (BRIN), South Tangerang, Indonesia
[2]Department of Geological Engineering, Faculty of Earth Technology and Energy, Universitas Trisakti, Jakarta, Indonesia

*E-mail: tyto001@brin.go.id

Article received: (received date), revised: (revised date), accepted:(accepted date) → **filled by Editor**

## ABSTRACT

Uranium and rare earth elements (REE) are essential elements for the development of green environmentally friendly, and sustainable energy. To meet the increasing demand for these raw materials, Indonesia has taken steps to explore and map potential deposits, including the Rirang Sector in Melawi Regency, West Kalimantan. However, the available information on the mineralization of these elements in the area is limited. Therefore, this study aimed to provide a detailed characterization on the petrology and geochemical characteristics of uranium ore and to synthesize the mineral genesis of uranium and REE-bearing ore in the Rirang Sector. The analytical methods used included petrography, micro-XRF, and geochemical analysis. The results showed that uranium mineralization was present in brannerites, uranophane, and swamboite associated with tourmaline and monazite ore. Similarly, REE concentrations were hosted by REE-bearing minerals, such as monazite, xenotime, and loparite. Geochemically, the uranium concentration in the monazite ore ranged from 1,110–28,440 ppm, while the total REE (TREE) concentration varied between 85,320 to 138,488 ppm. The formation of uranium and REE mineralization were due to the metasomatism process and its association with the Na-rich fluid of felsic intrusion. Notably, the weathering process did not enrich uranium and REE content in the soil but rather decreased it due to the leaching process and the absence of clay minerals capable of absorbing the REE cations on the surface of clay crystal structures.

**Keywords:** monazite, rare earth elements, tourmaline, uranium, West Kalimantan

## INTRODUCTION

Developing clean and efficient technologies is imperative to reduce carbon emissions and combat global warming, specifically as technology continues to advance rapidly. While renewable energy sources such as solar, hydro, and wind power are being prioritized in Indonesia, nuclear energy presents as a viable option for generating green energy. Developing those energy sources requires critical materials such as uranium for the nuclear fuel and rare earth elements (REE) for the MiMH battery component.

The exploration of uranium and REE is necessary to prepare the raw component for developing green and clean energy. One promising prospect of uranium and REE in Indonesia is located in Kalan Area, Melawi Regency, West Kalimantan [1], [2]. Some sectors in the Kalan area with uranium and REE potential are Tanah Merah, Jeronang, Indramayu, Jumbang, Dendang Arai, and Rirang [2]. In the Rirang Sector, uranium and REE-bearing ore consist of monazite and tourmaline ore. The average total rare earth oxides (REO) in monazite ore is 62,74%, and in tourmaline, the REO is 3.62% [2]. Uranium and REE resources in the Rirang area are estimated at approximately 227 tonnes of uranium and 3,917.59 tonnes of REO [2].

Mineralization signatures in the Rirang area consist of uraninite, monazite, tourmaline, pyrite, ilmenite, ilmenorutile, xenotime, and apatite [1], [3]–[5]. However, there is no other study on the distribution of the ore mineralization for the coeval REE and uranium. Therefore, this study aims to characterize the ore's petrology and geochemical characteristics and synthesize the mineral genesis of uranium and REE-bearing ore in the Rirang Sector, West Kalimantan.

## REGIONAL GEOLOGY

The Kalan area is occupied by predominant metamorphic, metasedimentary, intrusive, and volcanic rocks. Metamorphic rocks include quartzite, hornfels, and mica schist. These rocks are composed of quartz, biotite, and muscovite with accessory minerals such as tourmaline, andalusite, corundum, stilpnomelane, pyrophyllite, molybdenite, epidote, and sericite. The metasedimentary rocks consist of Jeronang metasiltstone, metasiltstone, meta-argillite, Jeronang metapelite, tuffaceous metapelite, and interbedding metasiltstone and metapelite. The metasiltstone-metapelite interbedding mainly hosts uranium ore in the Kalan area (Figure 1) [1], [2], [4]–[6].

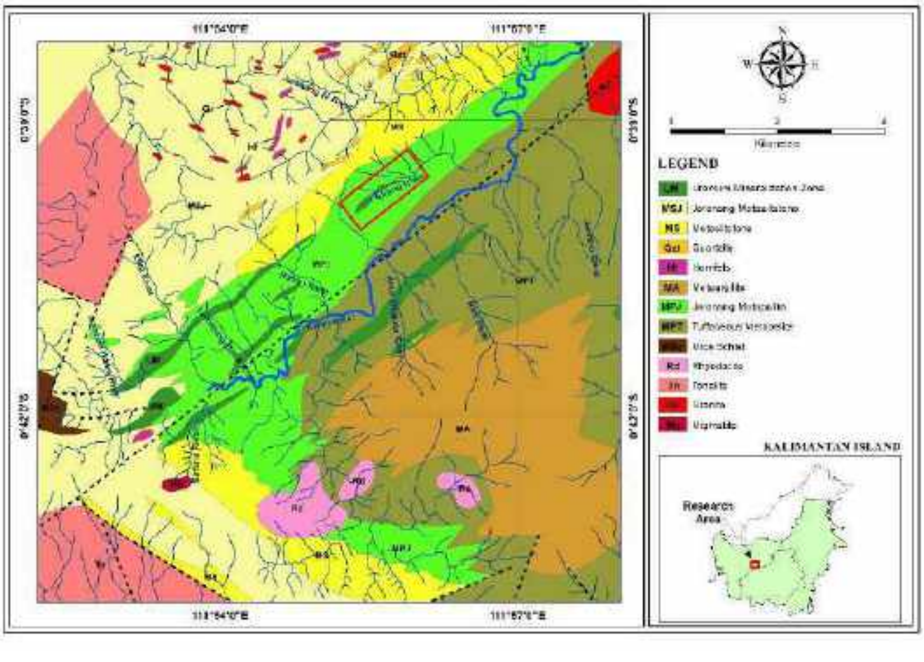

Figure 1. Geological Map of the Kalan Area, West Kalimantan. The Rirang Sector consists of the Jeronang Metapelite and Uranium Mineralization Zone (modified from[1], [2])

The metamorphic and metasedimentary rocks in the Kalan area were intruded by Sukadana Granite, Sepauk Tonalite, and Rhyodacite volcanic rocks. Both Sukadana Granite and Sepauk Tonalites are classified as Cretaceous intrusive rocks. Meanwhile, Rhyodacite volcanic is classified as Oligocene to Miocene Sintang Intrusive rock. Sukadana Granite is composed of quartz, orthoclase, plagioclase, biotite, zircon, and epidote. Sepauk Tonalite is primarily composed of biotite, hornblende, and plagioclase. Rhyodacite volcanic rock in the area consists of biotite, hornblende, oligoclase, andesine, and quartz, with some being shallow intrusions of sill or dike [1], [2].

The Rirang Sector consists of frequently weathered metasiltstone and metapelite. The bedding orientation is NNE-SSW and dipping 77°–86° directing to WNW [3], [4]. The foliation structure is ENE-WSW oriented with a dip of 40°–84° to NNW[3]. Subsequently, metasiltstone is generally composed of quartz and feldspar, with a minor amount of biotite and muscovite. The alteration minerals found in metasiltstone are chlorite, sericite, tourmaline, pyrite, and hematite. The metapelite exhibits a spotted shale texture with a unidirectional foliation structure. The spotted shale texture is interpreted as andalusite altered to fine sericite, muscovite, and quartz minerals. The metasiltstone and metapelite rocks are classified as greenschist facies[5].

The ore mineralization in the Rirang Sector is mainly found in boulder size and classified into two groups, tourmaline ore boulder and monazite ore boulder. Uranium and REE-bearing minerals consist of uraninite, brannerite, monazite, and xenotime. These minerals are associated with other ore minerals such as molybdenite, ilmenorutile, ilmenite, tourmaline, and apatite [5].

## METHODOLOGY

Samples were collected from the field along the Rirang River and represented by barren host rock, monazite ore, tourmaline ore, and weathered soil derived from monazite ore (Table 1). A total of 16 samples consisting of 2 barren host rocks, 7 monazite ores, 1 tourmaline ore, and 6 weathered soils were analyzed. This investigation's analytical methods included petrography, micro-XRF, and geochemical analysis. Petrography analysis was conducted using Leitz Laborlux 11 Pol and Nikon Eclipse E200 Polarization Microscope at Trisakti University, Indonesia. A total of 8 were analyzed petrographically to define the mineral composition, texture, and characteristics.

Table 1. Sample types and analyses.

| **No.** | **Sample Code** | **Sample Type** | **Analyses** | | |
|---|---|---|---|---|---|
| | | | **Petrography** | **Micro-XRF** | **XRF and ICP-MS** |
| 1 | RR02.3 | Host Rock | x | x | |
| 2 | RR09 | Host Rock | x | x | x |
| 3 | RR02 | Tourmaline Ore | x | x | |
| 4 | RR04 | Monazite Ore | x | x | |
| 5 | RR07 | Monazite Ore | x | x | x |
| 6 | RR10 | Monazite Ore | x | x | |
| 7 | RR13 | Monazite Ore | | | x |
| 8 | RR17 | Monazite Ore | x | x | |
| 9 | RR18 | Monazite Ore | | | x |
| 10 | RR23 | Monazite Ore | x | x | |
| 11 | RHS03 | Soil | | | x |
| 12 | RHS05 | Soil | | | x |
| 13 | RHS07 | Soil | | | x |
| 14 | RHS09 | Soil | | | x |
| 15 | RHS11 | Soil | | | x |
| 16 | RHS15 | Soil | | | x |

Notes: x denotes the performed analysis

Micro-XRF analysis was used to identify the elemental distribution in ore and host rock. This analysis was conducted using Bruker M4 Tornado Plus available in The Research Centre for Nuclear Fuel Cycle and Radioactive Waste Technology, The National Research and

Innovation Agency, Indonesia. A total of 8 ore and host rock samples were prepared in the form of a 5 x 5 cm smooth surface slab sample. During data acquisition, a pixel size of 35 µm was used to analyze a total area of approximately 30 x 30 mm. The X-ray tube was operated at 50kV and 600 µA, and a pixel time of 12 ms/pixel. The resulting maps were processed using Bruker M4 Tornado software to extract the elemental map from the sample. The analysis was continued using Advanced Mineral Identification and Characterization System (AMICS) software to determine the mineralogical composition of the sample[7], [8].

The geochemical analysis involved applying X-ray Fluorescence (XRF) and Induced Couple Plasma-Mass Spectrometry (ICP-MS). The XRF was used to determine major oxide composition and ICP-MS to identify trace elements in the samples. A total of 10 samples were analyzed at Indomineral Research, Indonesia, using Bruker S8 Tiger II for XRF analysis and Agilent 7900 ICP-MS for ICP-MS analysis. In this study, both Micro-XRF and XRF were used, with the former providing an advantage in elemental mapping across the samples, while the latter offered higher accuracy in quantification. Therefore, the use of dual analyses, remains relevant in this investigation.

## RESULTS

### Mineralogy

The host rock sample RR02.3 is a metapelite showing phyletic foliation with epiblastic-hypidioblastic texture. Foliation structures are evidenced by the linear alignment of fine clays composed of illite, kaolinite, chlorite, and wonesite. The AMICS analysis confirms the linear orientation of illite, kaolinite, and chlorite, and also identified other mineral compositions, such as almandine, cordierite, andalusite, staurolite, and tourmaline (Figure 2), that are usually present in trace amounts. Host rock sample RR09 is identified as metasiltstone, with slaty cleavage with lepidoblastic and xenoblastic texture. The mineralogy of the sample is composed of muscovite, oligoclase, and illite. Muscovite alters to a clay mineral with weathering, and hematite is found as a vein. The AMICS analysis indicates that the clay minerals in the metasilt are montmorillonite, illite, chlorite, and kaolinite. Metasiltstone also contains beryl and tourmaline in very small amounts.

Tourmaline ore, represented by RR02, shows a tourmaline vein with a predominant mineral composition of wonesite and polycrystalline quartz (Figure 3). Apatite occupies the edge of the tourmaline vein, and monazite is identified as an accessory mineral in the sample. The ore minerals found in the sample are rutile, magnetite, ilmenite, and brannerite. Brannerite and monazite are identified as uranium and REE-bearing minerals in the tourmaline ore. The AMICS analysis shows that erlianite and apatite are formed and occupy the edge of the vein. Brannerite and uranophane are found in uranium-bearing veins and are associated with xenotime, monazite, and apatite.

The monazite ore is dominated by an ore body of monazite with a uranium-bearing vein that cross-cuts the ore body. Monazite occurs in the form of polycrystalline grain having irregular and sutured boundaries. Accessory minerals found in the monazite ore include apatite, xenotime, tourmaline, ilmenite, rutile, pyrite, molybdenite, magnetite, quartz, hornblende, chlorite, and hematite. The quartz crystals are found in between monazite crystals. Almandine, cordierite, sudoite, and copper mineral are identified using AMICS analysis.

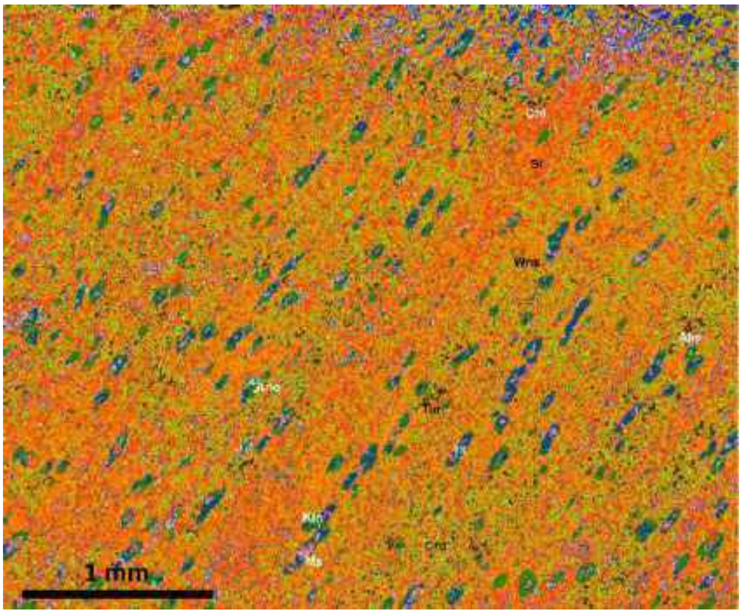

Figure 2. The AMICS results of metapelite host rock show spotted shale texture representing the foliation orientation. (Alm= almandine, Ano= anorthite, Chl= chlorite, Crd= cordierite, Ilt=illite, Kln=kaolinite, Ms=muscovite, St=staurolite, Wns=wonesite. The AMICS results of metapelite host rock show spotted shale texture representing the foliation orientation. (Alm= almandine, Ano= anorthite, Chl= chlorite, Crd= cordierite, Ilt=illite, Kln=kaolinite, Ms=muscovite, St=staurolite, Wns=wonesite. Mineral abbreviation after [9].

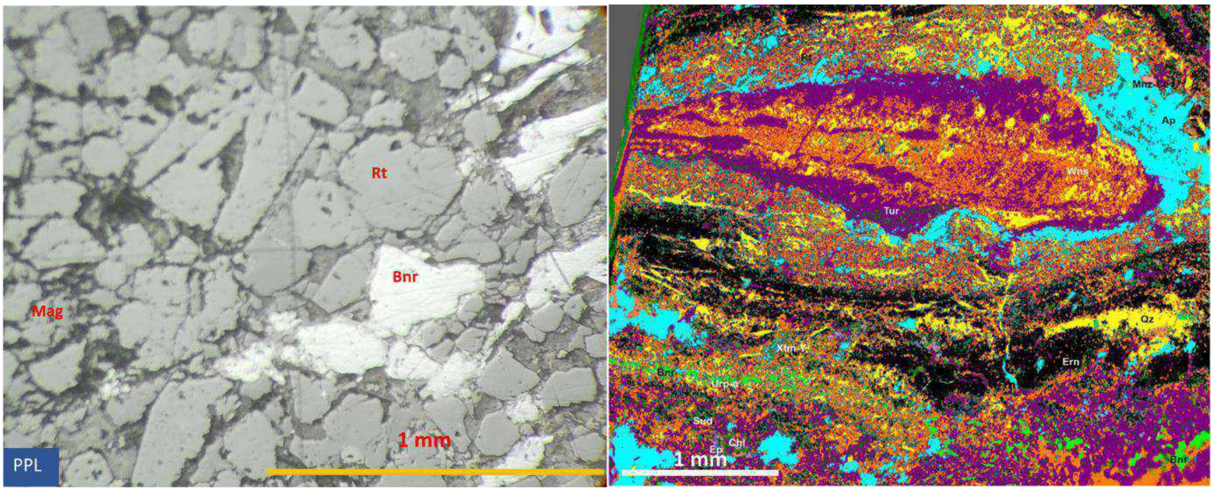

Figure 3. Microphotograph and AMICS result of tourmaline ore. Ore microphotograph shows brannerite as a uranium-bearing mineral associated with magnetite and rutile. AMICS result shows tourmaline vein associated with apatite, brannerite, and uranophane that cut the tourmaline ore (Ap= apatite, Bnr= brannerite, Chl= chlorite, Ep=epidote, Ern=erlianite, Mag = magnetite, Mnz-Ce=monazite-Ce. Qz=quartz, Rt=rutile, Sud=sudoite, Tur=tourmaline, Urp-α= uranophane, Xtm-Y= xenotime-Y. Mineral abbreviation after [9].

Uranium-bearing minerals found in the monazite ore are identified as brannerite and uranophane. These minerals are found in veins or spotted minerals associated with molybdenite, magnetite, rutile, ilmenite, and hematite. In addition, brannerite is found in prismatic form or irregular aggregates, despite a few brannerites occurring as deformed minerals (Figure 4). Molybdenites appear as irregular deformed-shaped inclusion of monazite. Based on AMICS analysis, swamboite presents as a secondary uranium-bearing mineral in the monazite ore.

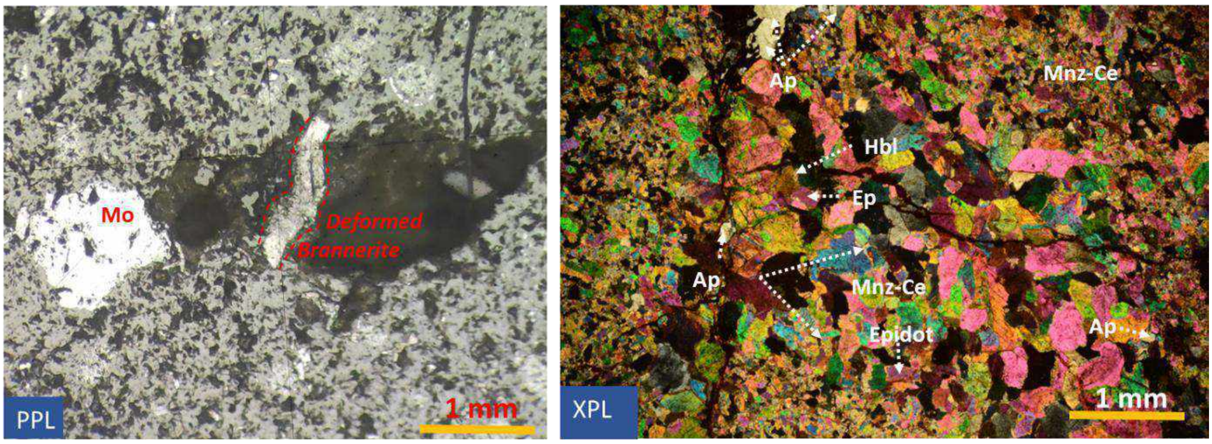

Figure 4. Microphotograph of monazite ore showing deformed brannerite, molybdenite, and polycrystalline monazite associated with apatite and epidote (Ap= apatite, Hbl= hornblende, Ep= epidote, Mnz-Ce = monazite, Rt= rutile, Mo= molybdenite. Mineral abbreviation after [9].

## Elemental Distribution

The elemental distribution of host rock samples (RR.02.3 and RR09) is predominated by Si, Al, Fe, and K (Figure 5). These elements usually occur in silicate minerals such as K-feldspar, mica, and clays. These elements form a clay mineral that dominates the host rock sample in the form of wonesite, illite, kaolinite, montmorillonite, and chlorite. Other minerals composed of these elements are muscovite, oligoclase, albite, biotite, staurolite, and cordierite.

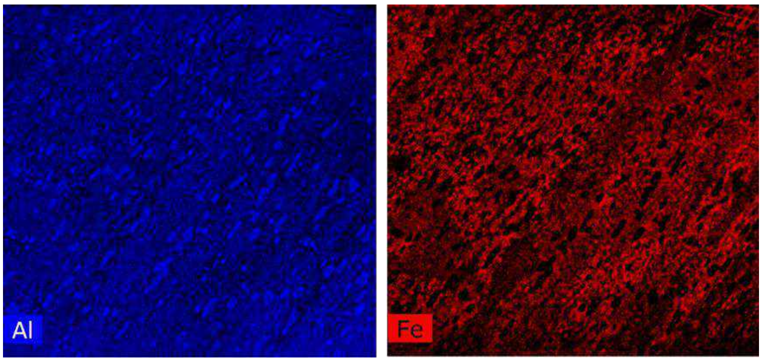

Figure 5. The distribution of dominant elements such as Al and Fe in the host rock sample indicates K-feldspar, mica, and clays distribution.

Uranium and REE are mainly found in the tourmaline and monazite ore samples. Si, Al, Fe, and Mg dominate the major element of tourmaline ore. These elements are found in tourmaline and wonesite minerals that are dominant in the sample. Uranium distribution in tourmaline ore concentrated along the veinlet associated with the Y element. The REE distribution can be divided into two groups, the Ce-Nd and Y groups. The Ce-Nd elements are closely associated and distributed randomly in the sample. On the other hand, Y is concentrated along the veinlet and at the edge of the tourmaline ore (Figure 6). The U-Y assemblages are incorporated in brannerite minerals, whereas Ce-Nd elements are incorporated in monazite, and Y s found in xenotime.

The elemental distributions in sample RR10, as monazite ore samples (Figure 7), are composed of Ce, La, P, and Nd, representing the monazite mineral. Uranium is distributed along the crack of the sample in the form of brannerite, uranophane, and swamboite minerals. The cracks are filled with elements such as Fe, Si, Cu, and Mo. The Fe is incorporated either in almandine or chlorite; Si represents quartz, Cu represents the occurrence of native copper, and Mo represents molybdenite. REE in the monazite ore sample includes Ce, La, Nd, Sm, Gd, and Y. The last element is the primary element found in xenotime. Furthermore, Gd occurs in trace amount and mainly form loparite mineral, and uranium distribution in monazite ore is associated with the Y element in several veins or cracks. But the other REE elements, such as Ce, La, Nd, Sm, and Gd are the dominant element across the samples, indicating that the monazite ore is formed before the uranium mineralization.

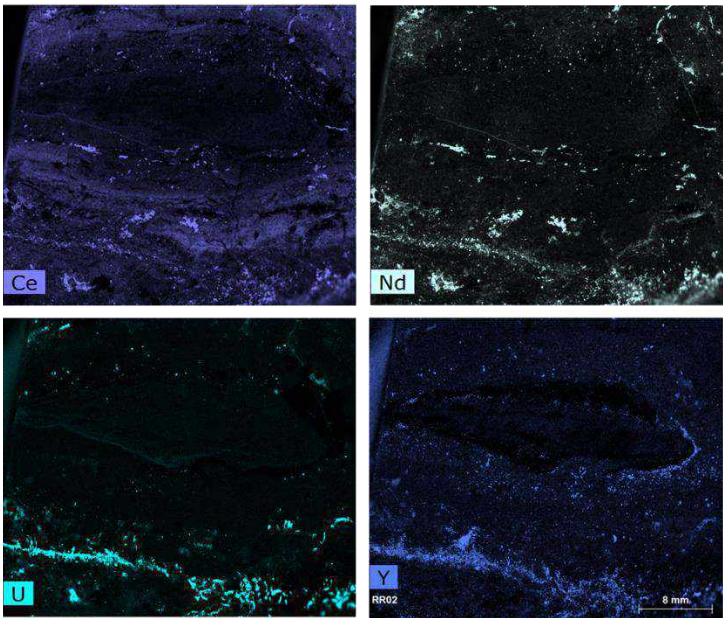

Figure 6. Distribution of uranium and REE in a tourmaline ore sample.

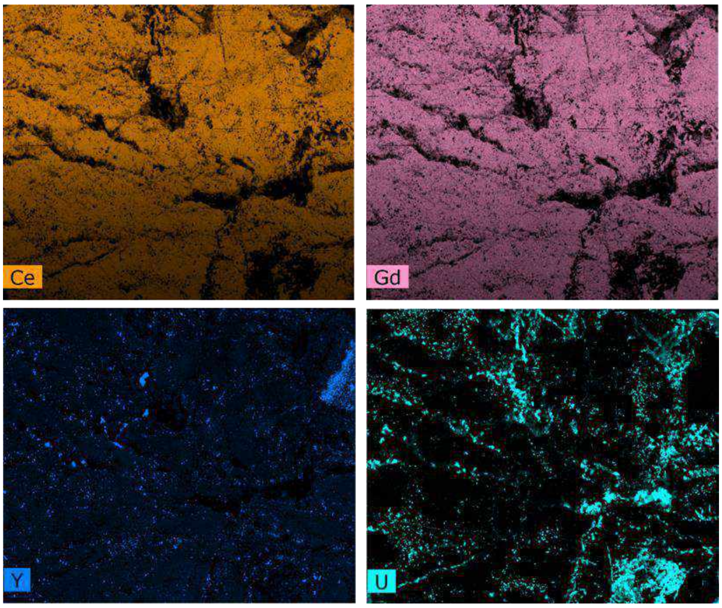

Figure 7. Distribution of uranium and REE in a monazite ore sample.

## Geochemistry

$SiO_2$ appears as the major element in the soil and host rock samples (ranges from 46.23 to 64.74%), much higher than the constituent in the monazite ore (1.46–16.73%). Subsequent major oxide compositions are $Fe_2O_3$, $Al_2O_3$, and $K_2O$ (Table 1). The silicate minerals dominate the soil and host rock and have undergone a weathering process, forming clays. In contrast, major oxides, such as CaO, MgO, MnO, $Cr_2O_3$, and $P_2O_5$, are relatively higher in monazite ore than in the soil or host rock sample. The presence of ore minerals such as monazite, apatite, and tourmaline cause the high concentration of these elements in monazite ore.

Table 2. Mayor oxide composition (wt.%) of soil, host rock, and monazite ore from the Rirang Sector.

| Element | Soil | | | | | | Host Rock | Monazite Ore | | |
|---|---|---|---|---|---|---|---|---|---|---|
| | RHS03 | RHS05 | RHS07 | RHS09 | RHS11 | RHS15 | RR09 | RR07 | RR13 | RR18 |
| $SiO_2$ | 49.29 | 60.21 | 64.74 | 49.77 | 46.23 | 50.06 | 61.93 | 7.67 | 16.73 | 1.46 |
| $Fe_2O_3$ | 9.31 | 7.10 | 12.17 | 8.27 | 13.65 | 12.81 | 7.14 | 2.19 | 3.03 | 1.13 |
| $Al_2O_3$ | 27.76 | 21.68 | 15.42 | 29.62 | 27.23 | 25.27 | 20.45 | 5.83 | 12.98 | 1.31 |
| CaO | <0.01 | <0.01 | <0.01 | <0.01 | <0.01 | <0.01 | 0.56 | 3.77 | 0.29 | 0.06 |
| MgO | 0.25 | 0.25 | 0.17 | 0.43 | 0.28 | 0.17 | 1.28 | 0.52 | 1.18 | 0.78 |
| MnO | <0.01 | <0.01 | 0.01 | 0.01 | 0.01 | 0.01 | 0.06 | 0.20 | 0.16 | 0.25 |
| $Cr_2O_3$ | 0.01 | 0.03 | 0.05 | 0.14 | 0.02 | 0.01 | 0.02 | 1.35 | 1.30 | 1.68 |
| $Na_2O$ | 1.28 | 1.05 | 0.74 | 2.25 | 1.07 | 1.31 | 1.74 | 1.90 | 1.63 | 1.38 |
| $K_2O$ | 4.39 | 1.75 | 0.51 | 6.09 | 2.67 | 3.44 | 2.65 | 2.71 | 2.55 | 0.53 |
| $TiO_2$ | 1.22 | 1.03 | 0.95 | 1.36 | 1.22 | 1.34 | 0.90 | 0.48 | 1.50 | 1.16 |
| $P_2O_5$ | 0.13 | 0.12 | 0.30 | 0.05 | 0.08 | 0.09 | 0.29 | 16.11 | 10.72 | 17.49 |
| LOI % | 8.42 | 8.38 | 7.21 | 7.35 | 10.31 | 7.67 | 4.45 | 2.55 | 3.32 | 0.87 |

The highest uranium concentration is found in monazite ore sample RR07, reaching 28,440 ppm, followed by other monazite ore RR18 (3,230 ppm), and RR13 (1,110 ppm). In the host rock sample, the uranium concentration reaches 391.96 ppm. In the soil sample, the uranium concentrations vary between 38.72–241.76 ppm (Table 3), indicating that the uranium element has leached out during weathering and is concentrated mainly in the ore body of monazite and tourmaline ores. The total REE (TREE) concentration in monazite ore is about 85,320–13,8488 ppm. REE in monazite ore is dominantly composed of light REE (LREE), with concentrations ranging from 81,813 to 133,772 ppm. Meanwhile, heavy REE (HREE) concentration ranges from 1,472 to 2,532 ppm (Table 4).

The variation diagram of uranium compared to several major oxides and trace elements (Figure 8) shows that uranium has a positive correlation with $Na_2O$ and $P_2O_5$, indicating that uranium-bearing minerals are chemically composed of elements such as brannerite, uranophane, swamboite, loparite, and monazite. The positive correlation between uranium and $P_2O_5$ also indicates that apatite and xenotime form co-genetically during uranium mineralization[10]. On the contrary, the negative correlation between uranium and $Al_2O_3$ and $Fe_2O_3$ indicates that uranium is not associated with silicate and ferrous minerals such as clays and ferromagnesian minerals.

Table 3. Trace elements composition (ppm) of soil, host rock, and monazite ore from the Rirang Sector.

| **Element** | **Soil** | | | | | | **Host Rock** | **Monazite Ore** | | |
|---|---|---|---|---|---|---|---|---|---|---|
| | **RHS03** | **RHS05** | **RHS07** | **RHS09** | **RHS11** | **RHS15** | **RR09** | **RR07** | **RR13** | **RR18** |
| Li | 15.9 | 12.0 | 5.0 | 16.0 | 18.7 | 17.9 | 47.5 | 3.4 | 15.8 | 2.9 |
| Be | 1.9 | 1.1 | 1.0 | 2.0 | 2.1 | 2.4 | 2.6 | 0.5 | 1.2 | 0.4 |
| V | 184.6 | 164.2 | 240.9 | 187.1 | 218.7 | 190.5 | 134.3 | 312.8 | 199.5 | 82.3 |
| Co | 8.4 | 8.7 | 9.2 | 6.0 | 8.7 | 8.9 | 37.6 | 2.6 | 4.8 | 1.2 |
| Ni | 74.0 | 59.2 | 154.8 | 48.8 | 90.4 | 126.0 | 75.1 | 1.5 | 6.5 | <0.001 |
| Cu | 40.5 | 34.5 | 78.5 | 29.3 | 35.2 | 48.5 | 34.8 | 3.4 | 112.1 | 24.9 |
| Zn | 11.2 | 9.6 | 15.8 | 12.1 | 10.3 | 4.2 | 56.9 | 5.2 | 4.5 | 0.2 |
| Ga | 38.1 | 30.9 | 35.0 | 36.2 | 35.2 | 38.9 | 58.6 | 879.7 | 1,087.7 | 1,582.4 |
| As | 16.5 | 19.8 | 15.0 | 14.3 | 20.8 | 15.0 | 27.1 | 189.7 | 312.8 | 516.9 |
| Se | 3.0 | 1.7 | 5.5 | 0.5 | 1.0 | 1.4 | 14.0 | 243.1 | 322.3 | 456.1 |
| Rb | 209.7 | 86.1 | 23.5 | 248.9 | 177.3 | 232.6 | 169.1 | 9.9 | 82.0 | 1.3 |
| Sr | 21.3 | 19.2 | 35.3 | 13.0 | 33.3 | 32.4 | 105.6 | 50.8 | 142.4 | 26.3 |
| Zr | 88.0 | 71.5 | 50.8 | 77.1 | 70.8 | 85.3 | 57.3 | 2.8 | 160.3 | 38.2 |
| Nb | 10.7 | 5.5 | 11.7 | 15.5 | 5.5 | 4.0 | 5.5 | 24.2 | 66.7 | 60.4 |
| Mo | 2,540.0 | 149.3 | 44.1 | 135.1 | 209.9 | 18.4 | 95.6 | 4,740.0 | 283.7 | 592.8 |
| Ag | 0.1 | 0.1 | 0.1 | 0.2 | 0.1 | 0.2 | 0.1 | 0.2 | 0.3 | 0.1 |
| Cd | 4.6 | 0.5 | 0.3 | 0.5 | 0.6 | 0.3 | 0.4 | 1.0 | 0.9 | 1.0 |
| Sn | 1.7 | 3.0 | 4.1 | 1.6 | 0.9 | 0.4 | 6.6 | 2.0 | 1.7 | <0.001 |
| Sb | 0.2 | 0.3 | 0.4 | 0.2 | 0.5 | 0.3 | 0.5 | 0.7 | 0.4 | 0.1 |
| Te | 0.2 | 0.2 | 0.2 | 0.1 | 0.1 | 0.1 | 0.1 | 0.4 | 0.4 | 0.2 |
| Cs | 3.8 | 2.8 | 1.4 | 3.9 | 5.7 | 6.4 | 6.5 | 0.5 | 0.9 | 0.2 |
| Ba | 481.8 | 250.2 | 77.2 | 568.4 | 281.1 | 372.6 | 316.6 | 53.2 | 575.4 | 17.9 |
| Hf | 2.5 | 2.2 | 1.9 | 2.4 | 1.9 | 2.5 | 2.0 | 11.8 | 14.4 | 18.4 |
| Ta | 0.9 | 0.7 | 1.1 | 1.3 | 0.5 | 0.5 | 0.7 | 2.1 | 2.9 | 3.0 |
| W | 4.7 | 3.4 | 6.5 | 5.5 | 2.1 | 1.3 | 3.4 | 19.7 | 39.0 | 13.8 |
| Pb | 59.7 | 25.2 | 115.2 | 27.6 | 6.7 | 6.9 | 88.2 | 3,840 | 1,260 | 1,550 |
| Bi | 0.3 | 0.4 | 0.5 | 0.2 | 0.2 | 0.2 | 0.4 | 0.4 | 0.6 | 0.2 |
| Th | 22.2 | 42.3 | 33.3 | 20.8 | 20.0 | 27.6 | 17.1 | 20.3 | 24.6 | 36.9 |
| U | 184.2 | 38.7 | 241.8 | 107.5 | 84.4 | 91.4 | 392.0 | 28,440.0 | 1,110.0 | 3,230.0 |

Table 4. REE composition (ppm) of soil, host rock, and monazite ore from the Rirang Sector.

| **Element** | **Soil** | | | | | | **Host Rock** | **Monazite Ore** | | |
|---|---|---|---|---|---|---|---|---|---|---|
| | **RHS03** | **RHS05** | **RHS07** | **RHS09** | **RHS11** | **RHS15** | **RR09** | **RR07** | **RR13** | **RR18** |
| La | 192.1 | 119.3 | 381.8 | 30.2 | 44.3 | 102.9 | 840.2 | 18,420 | 24,710 | 34,960 |
| Ce | 401 | 254.5 | 593.4 | 65.8 | 69.5 | 131.7 | 1,630 | 39,220 | 46,400 | > 50000 |
| Pr | 45.5 | 27.1 | 89.3 | 6.1 | 9.9 | 20.6 | 194.9 | 4,560 | 5,130 | 8,730 |
| Nd | 156.3 | 84.9 | 286.7 | 18.8 | 28.8 | 54.8 | 651.1 | 15,170 | 16,290 | 31,360 |
| Sm | 27.5 | 13.7 | 46.8 | 3.5 | 4.8 | 8.1 | 127.6 | 2,960 | 3,080 | 5,860 |
| Eu | 2.8 | 1.4 | 4.2 | 1 | 0.9 | 1.1 | 6.5 | 123.6 | 134.9 | 182 |
| Gd | 12.8 | 6.8 | 19.7 | 1.8 | 2.1 | 3.6 | 55.9 | 1,360.00 | 1,520.00 | 2,680.00 |
| Tb | 1.6 | 0.8 | 2.5 | 0.2 | 0.3 | 0.4 | 7.4 | 180.7 | 182.9 | 324.2 |
| Dy | 9.1 | 4.3 | 16.6 | 1.6 | 2.1 | 2.6 | 41.4 | 1,090.00 | 952.4 | 1,620.00 |
| Ho | 1.1 | 0.6 | 2.2 | 0.2 | 0.3 | 0.3 | 4.8 | 136.6 | 104.1 | 176.4 |
| Er | 2 | 1.1 | 3.9 | 0.6 | 0.7 | 0.8 | 8.3 | 239.4 | 149.4 | 257.9 |
| Tm | 0.3 | 0.1 | 0.4 | 0.1 | 0.1 | 0.1 | 0.9 | 27.4 | 13.9 | 24.8 |
| Yb | 1.6 | 1 | 2.3 | 0.7 | 0.9 | 0.9 | 4.8 | 140.9 | 57.3 | 106.3 |
| Lu | 0.2 | 0.1 | 0.3 | 0.1 | 0.1 | 0.1 | 0.7 | 19.7 | 12.1 | 22.8 |
| Sc | 28.4 | 23.8 | 30.3 | 35 | 36.4 | 32.6 | 22.3 | 32.4 | 20.5 | 4.7 |
| Y | 10.4 | 8.5 | 22.9 | 3.6 | 4.8 | 4.9 | 76.4 | 1,640.00 | 1,130.00 | 2,180.00 |
| TREE | 892.8 | 548.2 | 1,503.30 | 169.2 | 206 | 365.5 | 3,673.30 | 85,320.80 | 99,887.40 | 138,488.90 |
| $(La/Yb)_N$ | 79 | 84.1 | 113.7 | 30.3 | 34.9 | 80.3 | 118.7 | 88.3 | 291.3 | 222.3 |
| $(La/Sm)_N$ | 4.4 | 5.5 | 5.1 | 5.4 | 5.8 | 8 | 4.1 | 3.9 | 5 | 3.8 |
| $(Gd/Yb)_N$ | 6.3 | 5.8 | 7 | 2.2 | 2 | 3.4 | 9.5 | 7.8 | 21.5 | 20.4 |

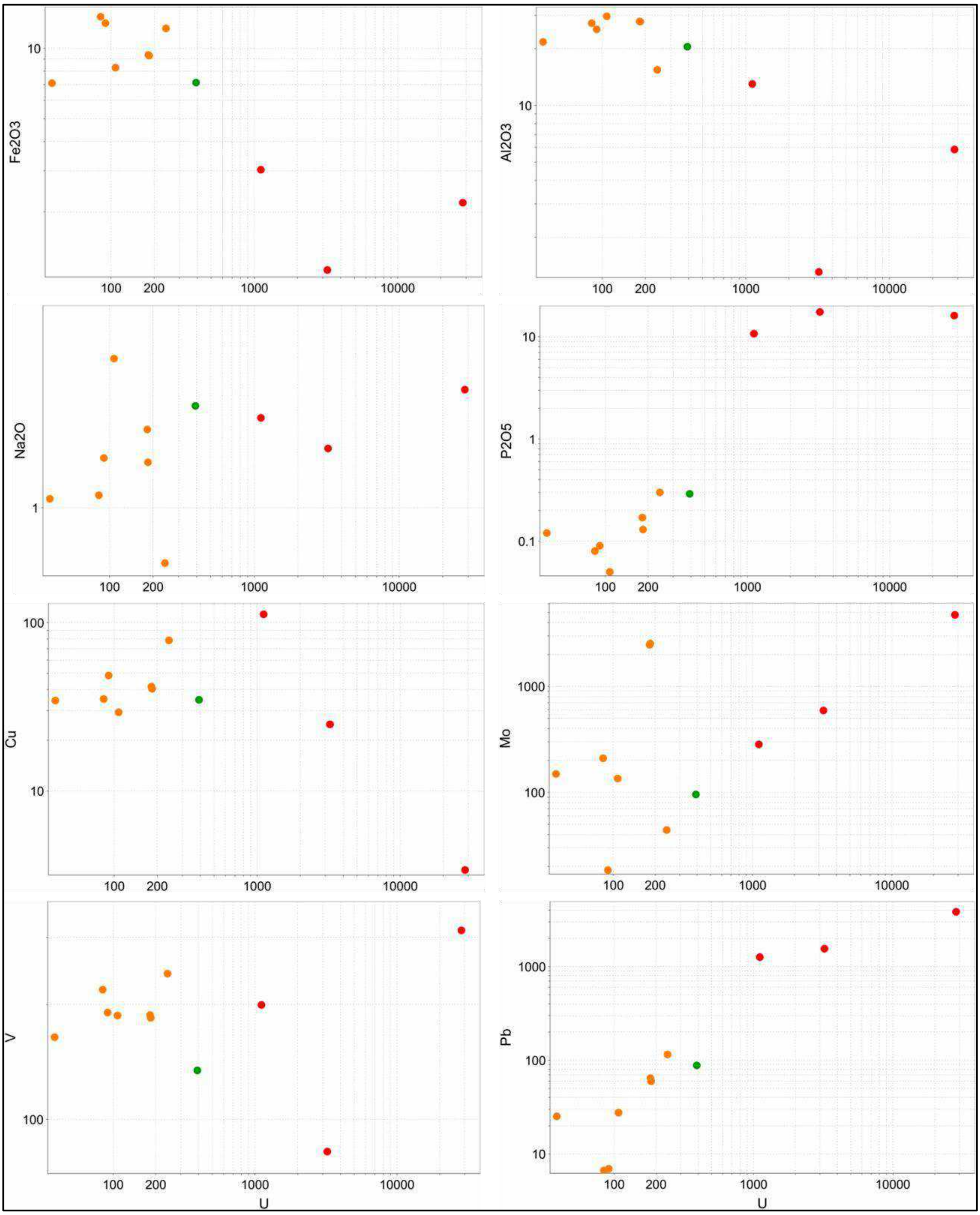

Figure 8. Variation diagram of uranium versus several major oxides and trace elements.

Compared to other elements, uranium exhibits a relatively strong positive correlation with marker elements of hydrothermal alteration products, including Cu, Mo, V, and Pb. Positive correlation suggests that these elements are enriched during the uranium mineralization process. U-Cu and U-Mo correlation shows relatively higher enrichment in the soil sample than other elements. Mo and Cu are believed to be adsorbed to the clay mineral during the weathering process. They are derived from the leaching process of host minerals, such as biotite, magnetite, hornblende K-feldspar, plagioclase, and ilmenite[11].

The variation diagram of TREE and several major oxides, uranium, and trace element (Figure 9) shows positive correlations with $Na_2O$ and $P_2O_5$, indicating that REE are mainly incorporated into phosphate or sodium oxide minerals as the REE-bearing minerals such as monazite, xenotime, apatite, and loparite. Mn oxide plays an important role in the distribution of REE because Mn oxides can bind REE through several processes, such as coprecipitation, adsorption, and ion exchange[12]. The $Na_2O$ and REE tend to become enriched in post-magmatic hydrothermal fluids. As a result, these elements are often closely associated with each other. On the other hand, TREE shows a negative correlation to $Al_2O_3$ and $Fe_2O_3$, indicating that REE is not enriched in clay-rich rocks or highly weathered soil. TREE shows a positive correlation compared to uranium and other trace elements such as Cu, V, and Pb. The data indicate that TREE and uranium are co-genetically concentrated during hydrothermal alteration.

The C1 Chondrite normalization[13] in the trace element diagram (Figure 10a) shows that the HFSE and LILE exhibited a greater depletion pattern than the Upper Continental Crust (UCC)[14] and the Post Archean Australian Shale (PAAS) [15]. On the other hand, uranium and REE show enrichment patterns, except for Eu, which shows depletion. The Eu depletion, followed by Sr and K depletion, indicates the weathering process of plagioclase[16]. In addition, the Eu depletion also indicates plagioclase fractionation in the magma source[12], [14].

The multi-element diagram of the REE-C1 chondrite (Figure 10b) shows an LREE enrichment and an HREE depletion pattern. These patterns indicate two alteration types during the uranium mineralization process, K-feldspar alteration and silicification[17], [18]. These patterns are also similar to the typical monazite that probably act as the main source of REE analyzed in the sample. The REE pattern in the soil sample shows similarity to the ore and host rock sample but has a lower value. The lower value indicates an early leaching phase of weathering process[19], [20].

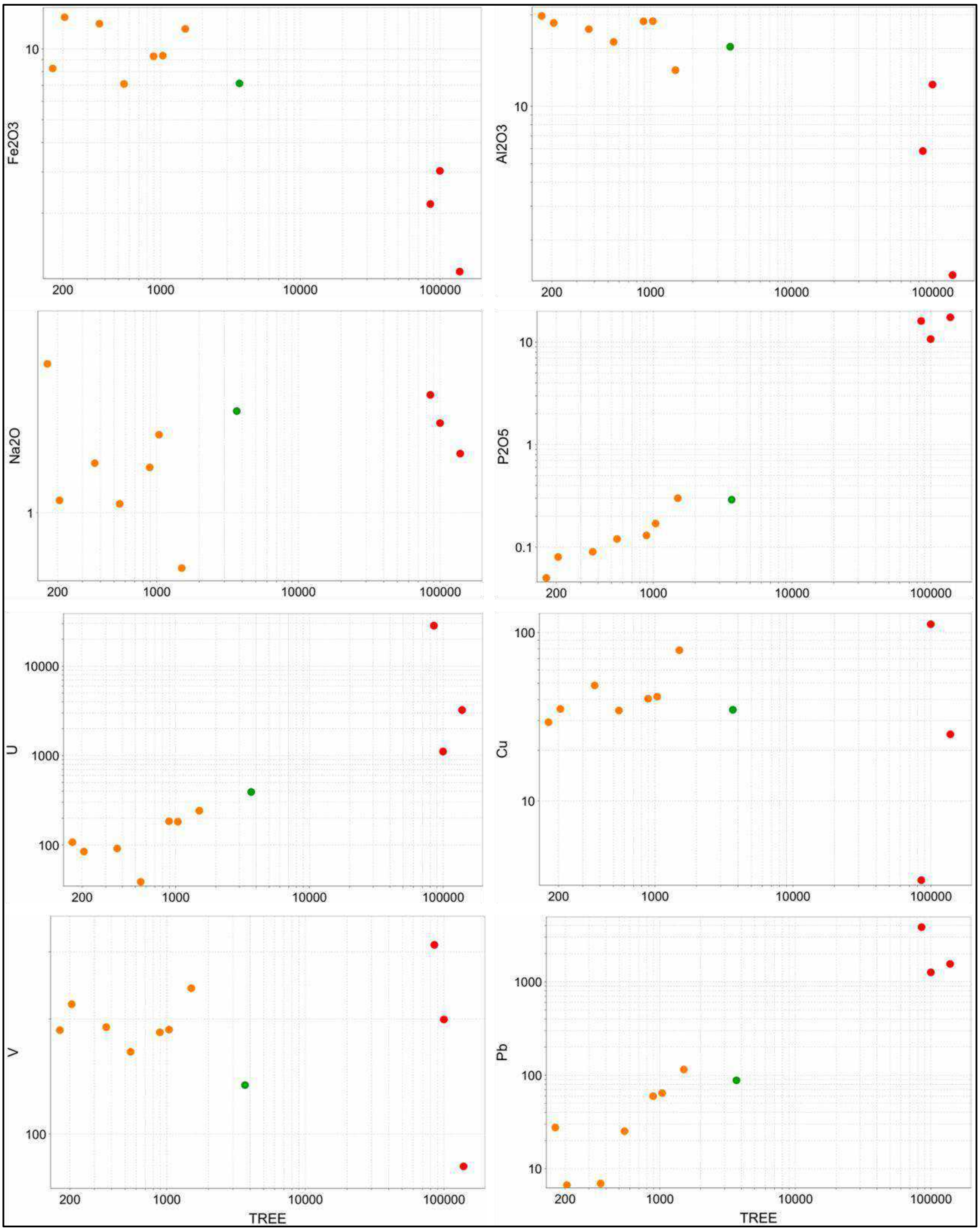

Figure 9. Variation diagram of TREE versus several major oxides and trace elements.

*p*-ISSN 0854-1418
*e*-ISSN 2503-426X

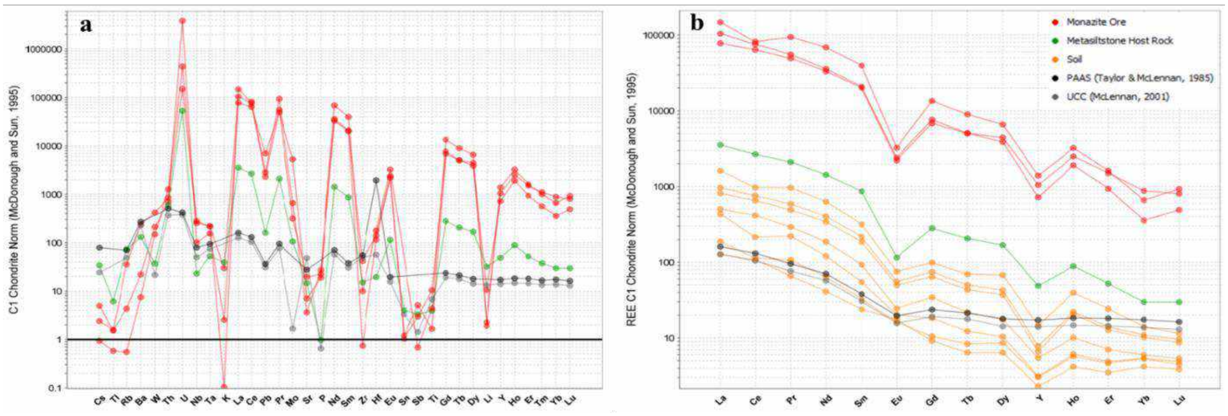

Figure 10. The multi-element plot of monazite ore, host rock, and soil in the Rirang Sector, West Kalimantan. a) Monazite ore and metasiltstone host rock show a depletion pattern in HSFE and LILE and enrichment in uranium and REE. b) Monazite ore, host rock, and soil show enrichment patterns in LREE and depletion patterns in HREE.

## DISCUSSION

The host rock for uranium and REE mineralization in the Rirang Sector are metamorphic rocks, including metapelite and metasiltstone. The metamorphic rocks were characterized by slaty to phyllitic foliation and spotted shale textures. The spotted shale texture is a result of clay minerals from weathered andalusite minerals, like wonesite and kaolinite. The occurrences of almandine, cordierite, and staurolite minerals indicate the regional metamorphism process. Paragenesis consisting of muscovite, almandine, and andalusite minerals indicates that the area's metamorphism facies were greenschist facies.

The rocks' REE pattern and Eu anomaly indicate the source rock characteristics[15]. A high LREE/HREE ratio and negative Eu anomaly are commonly found in granitic rocks[21]–[23]. The C1 Chondrite normalized REE plot shows a fractionated REE pattern ($(La/Yb)_N$ = 88.31–291.34, mean = 180.15), characterized by highly fractionated LREE ($(La/Sm)_N$ = 3.75–5.05, mean = 4.21) and HREE ($(Gd/Yb)_N$ = 7.82–21.49, mean = 14,8). In addition, REE pattern shows negative Eu anomaly, positive Ce anomaly, and enriched LREE/HREE ratio. This suggests that meta-siltstone and monazite ore are derived from felsic source rocks [24]. The granite intrusions north of the Rirang Sector (Figure 1) are strongly expected as a source of uranium and REE-bearing fluid. Uranium, REE, and several trace elements are commonly soluble in Na-rich rather than K-rich fluid. The occurrences of oligoclase and albite in the tourmaline and monazite ore characterize the Na-rich fluids. Moreover, Na-rich calc-silicate minerals such as hornblende associated with albite and oligoclase indicated the occurrence of sodic alteration [25]. On the other hand, the mineralization of brannerite, uranophane, and swamboite also indicated that the Na-metasomatism process occurred at medium temperatures [26]–[29]. The source of this metasomatism process is due to granitic intrusion in the north of the Rirang Sector and regionally correlated as Sukadana Granite.

The Rirang Sector is characterized by various mineralization and alteration processes that form several uranium and REE-bearing minerals, such as brannerite, uranophane, swamboite, monazite, xenotime, apatite, and loparite. Monazite, xenotime, apatite, and loparite are dominant LREE host minerals among these minerals. The high LREE/HREE ratio and negative Eu anomaly observed in the monazite ore indicated that these minerals originated from the felsic igneous source rocks.

In the samples studied, brannerite is the primary uranium-bearing mineral. This mineral cross-cuts the tourmaline and monazite ore, indicating that brannerite is formed in a later phase than both ores. Subsequently, brannerite is associated with pyrite, molybdenite, ilmenite, magnetite, rutile, and hematite, indicating the occurrence of the hydrothermal process during mineralization. Swamboite and uranophane are the later uranium mineral that formed resulting from the groundwater oxidation of brannerite [30].

The soil in the Rirang Sector, produced through weathering processes, exhibits a similar REE pattern to the host rocks and monazite ore. This similar pattern indicates an early phase leaching process of the monazite ore and host rock due to weathering [19], [20]. In some cases, weathering process can enrich the REE content in the soil [17], [28], [29], [31], with the main factor controlling the enrichment being clay minerals such as smectite, illite, kaolinite, and halloysite that act as adsorption agent of REE ions [19], [20], [32], [33]. In the Rirang sector, the clay mineral products are wonesite, illite, and kaolinite. Hence, the REE ions leach into the groundwater.

## CONCLUSION

The Rirang Sector in West Kalimantan contains metapelite and metasiltstone that contain uranium and rare earth element (REE) mineralization. The dominant clay minerals in these rocks are derived from volcanic sources, and the alteration minerals are a product of hydrothermal alteration. Tourmaline and monazite ores are associated with uranium and REE mineralization. On the other hand, REE mineralization occurs in the form of monazite, xenotime, and loparite. The enrichment of uranium, REE, and other trace elements are believed to be due to their association with the Na-rich fluid of felsic intrusion. The north of the Rirang Sector's felsic intrusions correlates with the Sukadana Granite on the regional scale. The enrichment process of REE is apparently due to the fractional crystallization of felsic fluid forming monazite, xenotime, apatite, and loparite. Furthermore, uranium enrichment is related to hydrothermal alteration, forming brannerite, uranophane, and other alteration minerals such as molybdenite, pyrite, copper, rutile, ilmenite, and magnetite. The interaction of the uranium-bearing mineral and groundwater forms secondary uranium mineral swamboite. The weathering process does not enrich the uranium and REE content in the soil but tend to decrease due to the leaching process and the absence of clay minerals that capable of binding REE ions into the soil.

## ACKNOWLEDGMENT

The authors are grateful to the National Research and Innovation Agency for providing the funding and facility to conduct this investigation. We also thank the anonymous reviewers for their thorough reviews and helpful suggestions.

## REFERENCES

[1] Ngadenin, A. Sumaryanto, H. Syaeful, and I. G. Sukadana, “Geologi dan Mineralisasi Uranium di Daerah Kalan, Kabupaten Melawi, Kalimantan Barat,” in *Seminar Nasional Kebumian XII*, Yogyakarta: Fakultas Teknologi Mineral, Universitas Pembangunan Nasional “Veteran” Yogyakarta, 2017, pp. 108–114.

[2] Ngadenin, I. G. Sukadana, and R. Fauzi, “Preliminary overview of the prospects for rare earth elements in Kalan , West Kalimantan , Indonesia Preliminary Overview of The Prospects for Rare Indonesia,” in *AIP Conference Proceedings*, 2022, pp. 1–11.

[3] Suharji, Ngadenin, Wagiyanto, and Sumarno, “Peningkatan Kwalitas Estimasi Cadangan

Uranium dan Unsur Tanah Jarang Sebagai Asosiasinya di Sektor Rirang Hulu, Kalimantan Barat," *Pros. Semin. IPTEK Nukl. dan Pengelolaan Sumber Daya Tambang*, pp. 51–65, 2002.

[4] S. Tjokrokardono, "Studi Provinsi Uranium Kalimantan; Kajian Mineralisasi Uranium Pada Batuan Metamorf Dan Granit Di Pegunungan Schwaner," *Seminar IPTEK Nuklir dan Pengelolaan Sumber Daya Tambang*. 2002.

[5] S. Tjokrokardono, L. Subiantoro, and M. Widodo, "Sintesis Geologi dan Mineralisasi Uranium Kalan dan Sekitarnya, Kalimantan Barat," Jakarta, 2006.

[6] B. Soetopo, R. Witjahyati, and Y. Wusana, "Sintesa Geologi dan Pemineralan Uranium Sektor Rabau Hulu, Kalan, Kalimantan Barat," *Semin. Geol. Nukl. dan Sumberd. Tambang Tahun 2004*, pp. 85–99, 2004.

[7] D. Savira, M. A. Gunawan, W. A. Draniswari, I. G. Sukadana, and F. Sihombing, "µxRF Application for Uranium Exploration (Case Study: Mamuju Deposit, Indonesia)," *IOP Conf. Ser. Earth Environ. Sci.*, vol. 830, no. 1, 2021, doi: 10.1088/1755-1315/830/1/012076.

[8] I. G. Sukadana, I. W. Warmada, F. Pratiwi, A. Harijoko, T. B. Adimedha, and A. W. Yogatama, "Elemental Mapping for Characterizing of Thorium and Rare Earth Elements (REE) Bearing Minerals Using µXRF," *Atom Indones.*, vol. 48, no. 2, pp. 87–98, 2022, doi: 10.17146/aij.2022.1215.

[9] L. N. Warr, "IMA–CNMNC approved mineral symbols," *Mineral. Mag.*, vol. 85, no. 3, pp. 291–320, 2021, doi: 10.1180/mgm.2021.43.

[10] P. Alexandre, "Mineralogy and geochemistry of the sodium metasomatism-related uranium occurrence of Aricheng South, Guyana," *Miner. Depos.*, vol. 45, no. 4, pp. 351–367, 2010, doi: 10.1007/s00126-010-0278-7.

[11] J. A. Plant, P. R. Simpson, B. Smith, and B. F. Windley, "Uranium ore deposits-products of the radioactive earth," *Uranium Mineral. Geochemistry, Environ.*, no. September, pp. 255–319, 2019, doi: 10.1515/9781501509193-011.

[12] X. P. Yan, R. Kerrich, and M. J. Hendry, "Sequential leachates of multiple grain size fractions from a clay-rich till, Saskatchewan, Canada: Implications for controls on the rare earth element geochemistry of porewaters in an aquitard," *Chem. Geol.*, vol. 158, no. 1–2, pp. 53–79, 1999, doi: 10.1016/S0009-2541(99)00011-X.

[13] W. F. McDonough and S. s. Sun, "The composition of the Earth," *Chem. Geol.*, vol. 120, no. 3–4, pp. 223–253, 1995, doi: 10.1016/0009-2541(94)00140-4.

[14] S. M. McLennan, "Relationships between the trace element composition of sedimentary rocks and upper continental crust," *Geochemistry, Geophys. Geosystems*, vol. 2, 2001, doi: 10.1038/scientificamerican0983-130.

[15] S. R. Taylor and S. M. McLennan, *The continental crust: Its composition and evolution*. 1985.

[16] C. Wang, L. Zhang, Y. Dai, and C. Lan, "Geochronological and geochemical constraints on the origin of clastic meta-sedimentary rocks associated with the Yuanjiacun BIF from the Lüliang Complex, North China," *Lithos*, vol. 212–215, pp. 231–246, 2015, doi: 10.1016/j.lithos.2014.11.015.

[17] Z. Bao and Z. Zhao, "Rare-earth element mobility during ore-forming hydrothermal alteration: A case study of Dongping gold deposit, Hebei Province, China," *Chinese J. Geochemistry*, vol. 22, no. 1, pp. 45–57, 2003, doi: 10.1007/bf02831545.

[18] S. Akhtar, X. Yang, and F. Pirajno, "Sandstone type uranium deposits in the Ordos Basin, Northwest China: A case study and an overview," *J. Asian Earth Sci.*, vol. 146, no. September 2016, pp. 367–382, 2017, doi: 10.1016/j.jseaes.2017.05.028.

[19] Y. Kanazawa and M. Kamitani, "Rare earth minerals and resources in the world," in *Journal of Alloys and Compounds*, Feb. 2006, pp. 1339–1343. doi: 10.1016/j.jallcom.2005.04.033.

[20] A. Berger, E. Janots, E. Gnos, R. Frei, and F. Bernier, "Rare earth element mineralogy and geochemistry in a laterite profile from Madagascar," *Appl. Geochemistry*, vol. 41, pp. 218–228, 2014, doi: 10.1016/j.apgeochem.2013.12.013.

[21] G. W. A. Nyakairu and C. Koeberl, "Mineralogical and chemical composition and distribution of rare earth elements in clay-rich sediments from central Uganda," *Geochem. J.*, vol. 35, no. 1, pp. 13–28, 2001, doi: 10.2343/geochemj.35.13.

[22] B. K. Das, A. S. AL-Mikhlafi, and P. Kaur, "Geochemistry of Mansar Lake sediments, Jammu, India: Implication for source-area weathering, provenance, and tectonic setting," *J. Asian Earth Sci.*, vol. 26, no. 6, pp. 649–668, 2006, doi: 10.1016/j.jseaes.2005.01.005.

[23] R. Kritsananuwat, S. K. Sahoo, M. Fukushi, and S. Chanyotha, "Distribution of rare earth elements, thorium and uranium in Gulf of Thailand's sediments," *Environ. Earth Sci.*, vol. 73, no. 7, pp. 3361–3374, 2015, doi: 10.1007/s12665-014-3624-8.

[24] D. Bakkiaraj, R. Nagendra, R. Nagarajan, and J. S. Armstrong-Altrin, "Geochemistry of sandstones from the upper Cretaceous sillakkudi Formation, Cauvery basin, Southern India: Implication for provenance," *J. Geol. Soc. India*, vol. 76, no. 5, pp. 453–467, 2010, doi: 10.1007/s12594-010-0128-3.

[25] R. G. Skirrow *et al.*, *Uranium Mineral Systems : Processes , exploration criteria and a new deposit framework*. Geosciences Australia Record 2009/20, 2009.

[26] A. D. Mckay and Y. Miezitis, "Australia's uranium resources, geology and development of deposits.," 2001. doi: 10.1159/000335161.

[27] P. A. Polito and T. K. Kyser, "The Valhalla Uranium Deposit, Qeensland, Australia," *ASEG Ext. Abstr.*, vol. 2006, no. 1, pp. 1–4, 2006, doi: 10.1071/aseg2006ab140.

[28] M. Cuney and K. Kyser, "Recent and not-so-recent developments in uranium deposits and implications for exploration," *Short Course Ser. Vol. 39*, vol. 39, no. January 2009, p. 259, 2008.

[29] M. Cuney, A. Emetz, J. Mercadier, V. Mykchaylov, V. Shunko, and A. Yuslenko, "Uranium deposits associated with Na-metasomatism from central Ukraine: A review of some of the major deposits and genetic constraints," *Ore Geol. Rev.*, vol. 44, pp. 82–106, 2012, doi: 10.1016/j.oregeorev.2011.09.007.

[30] P. Bruneton and M. Cuney, *Geology of uranium deposits*, no. 1956. Elsevier Ltd, 2016. doi: 10.1016/B978-0-08-100307-7.00002-8.

[31] M. Bau, "Rare-earth element mobility during hydrothermal and metamorphic fluid-rock interaction and the significance of the oxidation state of europium," *Chem. Geol.*, vol. 93, no. 3–4, pp. 219–230, 1991, doi: 10.1016/0009-2541(91)90115-8.

[32] G. Estrade, E. Marquis, M. Smith, K. Goodenough, and P. Nason, "REE concentration processes in ion adsorption deposits: Evidence from the Ambohimirahavavy alkaline complex in Madagascar," *Ore Geol. Rev.*, vol. 112, no. March, p. 103027, 2019, doi: 10.1016/j.oregeorev.2019.103027.

[33] D. Wang *et al.*, "Exploration and research progress on ion-adsorption type REE deposit in South China," *China Geol.*, vol. 1, no. 3, pp. 414–423, 2018, doi: 10.31035/cg2018022.

# Distribution and Characteristics of Rare Earth Elements in Uranium-Ore Deposits from Rirang Area, West Kalimantan Province, Indonesia

*by* Dita Dita

---

**Submission date:** 30-Jul-2024 07:03PM (UTC+0700)
**Submission ID:** 2424815365
**File name:** 7058-26774-1-PB.pdf (1.92M)
**Word count:** 6759
**Character count:** 33663

*Eksplorium*
Volume 45 No. 1, Mei/November 2024: 1–16

*p*-ISSN 0854-1418
*e*-ISSN 2503-426X

# Distribution and Characteristics of Rare Earth Elements in Uranium-Ore Deposits from Rirang Area, West Kalimantan Province, Indonesia

**Tyto Baskara Adimedha[1*], Rayhan Aldizan Farrenzo[2], I Gde Sukadana[1], Rosmalia Dita Nugraheni[2], Fadiah Pratiwi[1], Roni Cahya Ciputra[1], Frederikus Dian Indrastomo[1], Heri Syaeful[1], Yoshi Rachael[1]**

[1]Research Center for Nuclear Mineral and Radioactive Waste Technology, The National Research and Innovation Agency (BRIN), South Tangerang, Indonesia
[2]Department of Geological Engineering, Faculty of Earth Technology and Energy, Universitas Trisakti, Jakarta, Indonesia

*E-mail: tyto001@brin.go.id

Article received: (received date), revised: (revised date), accepted:(accepted date) → **filled by Editor**

## ABSTRACT

Uranium and rare earth elements (REE) are essential elements for the development of green environmentally friendly, and sustainable energy. To meet the increasing demand for these raw materials, Indonesia has taken steps to explore and map potential deposits, including the Rirang Sector in Melawi Regency, West Kalimantan. However, the available information on the mineralization of these elements in the area is limited. Therefore, this study aimed to provide a detailed characterization on the petrology and geochemical characteristics of uranium ore and to synthesize the mineral genesis of uranium and REE-bearing ore in the Rirang Sector. The analytical methods used included petrography, micro-XRF, and geochemical analysis. The results showed that uranium mineralization was present in brannerites, uranophane, and swamboite associated with tourmaline and monazite ore. Similarly, REE concentrations were hosted by REE-bearing minerals, such as monazite, xenotime, and loparite. Geochemically, the uranium concentration in the monazite ore ranged from 1,110–28,440 ppm, while the total REE (TREE) concentration varied between 85,320 to 138,488 ppm. The formation of uranium and REE mineralization were due to the metasomatism process and its association with the Na-rich fluid of felsic intrusion. Notably, the weathering process did not enrich uranium and REE content in the soil but rather decreased it due to the leaching process and the absence of clay minerals capable of absorbing the REE cations on the surface of clay crystal structures.

**Keywords:** monazite, rare earth elements, tourmaline, uranium, West Kalimantan

## INTRODUCTION

Developing clean and efficient technologies is imperative to reduce carbon emissions and combat global warming, specifically as technology continues to advance rapidly. While renewable energy sources such as solar, hydro, and wind power are being prioritized in Indonesia, nuclear energy presents as a viable option for generating green energy. Developing those energy sources requires critical materials such as uranium for the nuclear fuel and rare earth elements (REE) for the MiMH battery component.

The exploration of uranium and REE is necessary to prepare the raw component for developing green and clean energy. One promising prospect of uranium and REE in Indonesia is located in Kalan Area, Melawi Regency, West Kalimantan [1], [2]. Some sectors in the Kalan area with uranium and REE potential are Tanah Merah, Jeronang, Indramayu, Jumbang, Dendang Arai, and Rirang [2]. In the Rirang Sector, uranium and REE-bearing ore consist of monazite and tourmaline ore. The average total rare earth oxides (REO) in monazite ore is 62,74%, and in tourmaline, the REO is 3.62% [2]. Uranium and REE resources in the Rirang area are estimated at approximately 227 tonnes of uranium and 3,917.59 tonnes of REO [2].

Mineralization signatures in the Rirang area consist of uraninite, monazite, tourmaline, pyrite, ilmenite, ilmenorutile, xenotime, and apatite [1], [3]–[5]. However, there is no other study on the distribution of the ore mineralization for the coeval REE and uranium. Therefore, this study aims to characterize the ore's petrology and geochemical characteristics and synthesize the mineral genesis of uranium and REE-bearing ore in the Rirang Sector, West Kalimantan.

## REGIONAL GEOLOGY

The Kalan area is occupied by predominant metamorphic, metasedimentary, intrusive, and volcanic rocks. Metamorphic rocks include quartzite, hornfels, and mica schist. These rocks are composed of quartz, biotite, and muscovite with accessory minerals such as tourmaline, andalusite, corundum, stilpnomelane, pyrophyllite, molybdenite, epidote, and sericite. The metasedimentary rocks consist of Jeronang metasiltstone, metasiltstone, meta-argillite, Jeronang metapelite, tuffaceous metapelite, and interbedding metasiltstone and metapelite. The metasiltstone-metapelite interbedding mainly hosts uranium ore in the Kalan area (Figure 1) [1], [2], [4]–[6].

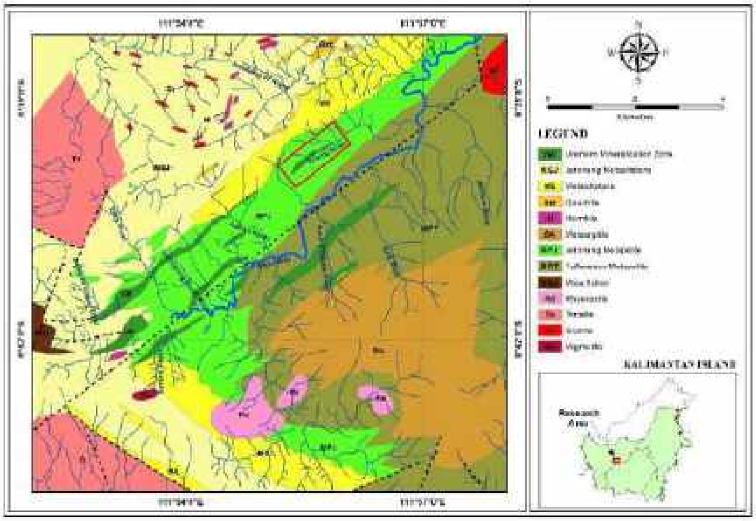

Figure 1. Geological Map of the Kalan Area, West Kalimantan. The Rirang Sector consists of the Jeronang Metapelite and Uranium Mineralization Zone (modified from[1], [2])

The metamorphic and metasedimentary rocks in the Kalan area were intruded by Sukadana Granite, Sepauk Tonalite, and Rhyodacite volcanic rocks. Both Sukadana Granite and Sepauk Tonalites are classified as Cretaceous intrusive rocks. Meanwhile, Rhyodacite volcanic is classified as Oligocene to Miocene Sintang Intrusive rock. Sukadana Granite is composed of quartz, orthoclase, plagioclase, biotite, zircon, and epidote. Sepauk Tonalite is primarily composed of biotite, hornblende, and plagioclase. Rhyodacite volcanic rock in the area consists of biotite, hornblende, oligoclase, andesine,

p-ISSN 0854-1418
e-ISSN 2503-426X

and quartz, with some being shallow intrusions of sill or dike [1], [2].

The Rirang Sector consists of frequently weathered metasiltstone and metapelite. The bedding orientation is NNE-SSW and dipping 77°–86° directing to WNW [3], [4]. The foliation structure is ENE-WSW oriented with a dip of 40°–84° to NNW[3]. Subsequently, metasiltstone is generally composed of quartz and feldspar, with a minor amount of biotite and muscovite. The alteration minerals found in metasiltstone are chlorite, sericite, tourmaline, pyrite, and hematite. The metapelite exhibits a spotted shale texture with a unidirectional foliation structure. The spotted shale texture is interpreted as andalusite altered to fine sericite, muscovite, and quartz minerals. The metasiltstone and metapelite rocks are classified as greenschist facies[5].

The ore mineralization in the Rirang Sector is mainly found in boulder size and classified into two groups, tourmaline ore boulder and monazite ore boulder. Uranium and REE-bearing minerals consist of uraninite, brannerite, monazite, and xenotime. These minerals are associated with other ore minerals such as molybdenite, ilmenorutile, ilmenite, tourmaline, and apatite [5].

## METHODOLOGY

Samples were collected from the field along the Rirang River and represented by barren host rock, monazite ore, tourmaline ore, and weathered soil derived from monazite ore (Table 1). A total of 16 samples consisting of 2 barren host rocks, 7 monazite ores, 1 tourmaline ore, and 6 weathered soils were analyzed. This investigation's analytical methods included petrography, micro-XRF, and geochemical analysis. Petrography analysis was conducted using Leitz Laborlux 11 Pol and Nikon Eclipse E200 Polarization Microscope at Trisakti University, Indonesia. A total of 8 were analyzed petrographically to define the mineral composition, texture, and characteristics.

Table 1. Sample types and analyses.

| No. | Sample Code | Sample Type | Analyses | | |
|---|---|---|---|---|---|
| | | | Petrography | Micro-XRF | XRF and ICP-MS |
| 1 | RR02.3 | Host Rock | x | x | |
| 2 | RR09 | Host Rock | x | x | x |
| 3 | RR02 | Tourmaline Ore | x | x | |
| 4 | RR04 | Monazite Ore | x | x | |
| 5 | RR07 | Monazite Ore | x | x | x |
| 6 | RR10 | Monazite Ore | x | x | |
| 7 | RR13 | Monazite Ore | | | x |
| 8 | RR17 | Monazite Ore | x | x | |
| 9 | RR18 | Monazite Ore | | | x |
| 10 | RR23 | Monazite Ore | x | x | |
| 11 | RHS03 | Soil | | | x |
| 12 | RHS05 | Soil | | | x |
| 13 | RHS07 | Soil | | | x |
| 14 | RHS09 | Soil | | | x |
| 15 | RHS11 | Soil | | | x |
| 16 | RHS15 | Soil | | | x |

Notes: x denotes the performed analysis

Micro-XRF analysis was used to identify the elemental distribution in ore and host rock. This analysis was conducted using Bruker M4 Tornado Plus available in The Research Centre for Nuclear Fuel Cycle and Radioactive Waste Technology, The National Research and

Innovation Agency, Indonesia. A total of 8 ore and host rock samples were prepared in the form of a 5 x 5 cm smooth surface slab sample. During data acquisition, a pixel size of 35 $\mu$m was used to analyze a total area of approximately 30 x 30 mm. The X-ray tube was operated at 50kV and 600 $\mu$A, and a pixel time of 12 ms/pixel. The resulting maps were processed using Bruker M4 Tornado software to extract the elemental map from the sample. The analysis was continued using Advanced Mineral Identification and Characterization System (AMICS) software to determine the mineralogical composition of the sample[7], [8].

The geochemical analysis involved applying X-ray Fluorescence (XRF) and Induced Couple Plasma-Mass Spectrometry (ICP-MS). The XRF was used to determine major oxide composition and ICP-MS to identify trace elements in the samples. A total of 10 samples were analyzed at Indomineral Research, Indonesia, using Bruker S8 Tiger II for XRF analysis and Agilent 7900 ICP-MS for ICP-MS analysis. In this study, both Micro-XRF and XRF were used, with the former providing an advantage in elemental mapping across the samples, while the latter offered higher accuracy in quantification. Therefore, the use of dual analyses, remains relevant in this investigation.

## RESULTS

### Mineralogy

The host rock sample RR02.3 is a metapelite showing phyletic foliation with epiblastic-hypidioblastic texture. Foliation structures are evidenced by the linear alignment of fine clays composed of illite, kaolinite, chlorite, and wonesite. The AMICS analysis confirms the linear orientation of illite, kaolinite, and chlorite, and also identified other mineral compositions, such as almandine, cordierite, andalusite, staurolite, and tourmaline (Figure 2), that are usually present in trace amounts. Host rock sample RR09 is identified as metasiltstone, with slaty cleavage with lepidoblastic and xenoblastic texture. The mineralogy of the sample is composed of muscovite, oligoclase, and illite. Muscovite alters to a clay mineral with weathering, and hematite is found as a vein. The AMICS analysis indicates that the clay minerals in the metasilt are montmorillonite, illite, chlorite, and kaolinite. Metasiltstone also contains beryl and tourmaline in very small amounts.

Tourmaline ore, represented by RR02, shows a tourmaline vein with a predominant mineral composition of wonesite and polycrystalline quartz (Figure 3). Apatite occupies the edge of the tourmaline vein, and monazite is identified as an accessory mineral in the sample. The ore minerals found in the sample are rutile, magnetite, ilmenite, and brannerite. Brannerite and monazite are identified as uranium and REE-bearing minerals in the tourmaline ore. The AMICS analysis shows that erlianite and apatite are formed and occupy the edge of the vein. Brannerite and uranophane are found in uranium-bearing veins and are associated with xenotime, monazite, and apatite.

The monazite ore is dominated by an ore body of monazite with a uranium-bearing vein that cross-cuts the ore body. Monazite occurs in the form of polycrystalline grain having irregular and sutured boundaries. Accessory minerals found in the monazite ore include apatite, xenotime, tourmaline, ilmenite, rutile, pyrite, molybdenite, magnetite, quartz, hornblende, chlorite, and hematite. The quartz crystals are found in between monazite crystals. Almandine, cordierite, sudoite, and copper mineral are identified using AMICS analysis.

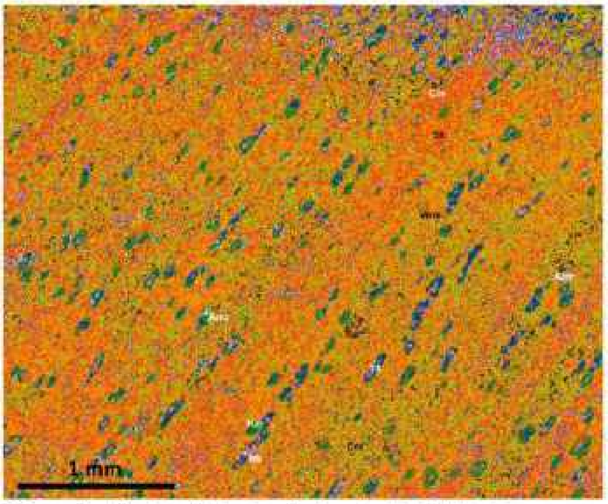

Figure 2. The AMICS results of metapelite host rock show spotted shale texture representing the foliation orientation. (Alm= almandine, Ano= anorthite, Chl= chlorite, Crd= cordierite, Ilt=illite, Kln=kaolinite, Ms=muscovite, St=staurolite, Wns=wonesite. The AMICS results of metapelite host rock show spotted shale texture representing the foliation orientation. (Alm=almandine, Ano= anorthite, Chl= chlorite, Crd=cordierite, Ilt=illite, Kln=kaolinite, Ms=muscovite, St=staurolite, Wns=wonesite. Mineral abbreviation after [9].

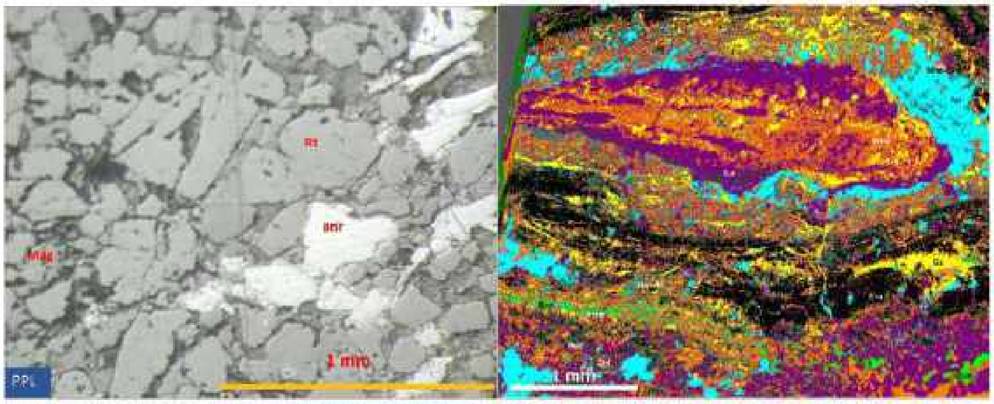

Figure 3. Microphotograph and AMICS result of tourmaline ore. Ore microphotograph shows brannerite as a uranium-bearing mineral associated with magnetite and rutile. AMICS result shows tourmaline vein associated with apatite, brannerite, and uranophane that cut the tourmaline ore (Ap= apatite, Bnr= brannerite, Chl= chlorite, Ep=epidote, Ern=erlianite, Mag = magnetite, Mnz-Ce=monazite-Ce, Qz=quartz, Rt=rutile, Sud=sudoite, Tur=tourmaline, Urp-α= uranophane, Xtm-Y= xenotime-Y. Mineral abbreviation after [9].

Uranium-bearing minerals found in the monazite ore are identified as brannerite and uranophane. These minerals are found in veins or spotted minerals associated with molybdenite, magnetite, rutile, ilmenite, and hematite. In addition, brannerite is found in prismatic form or irregular aggregates, despite a few brannerites occurring as deformed minerals (Figure 4). Molybdenites appear as irregular deformed-shaped inclusion of monazite. Based on AMICS analysis, swamboite presents as a secondary uranium-bearing mineral in the monazite ore.

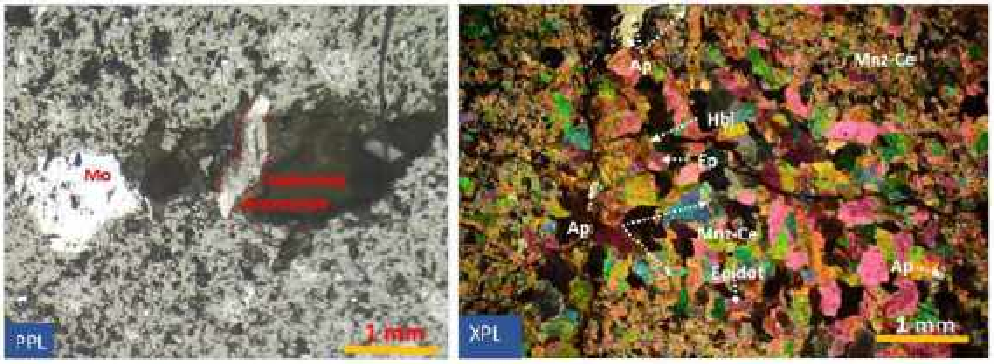

Figure 4. Microphotograph of monazite ore showing deformed brannerite, molybdenite, and polycrystalline monazite associated with apatite and epidote (Ap= apatite, Hbl= hornblende, Ep= epidote, Mnz-Ce = monazite, Rt= rutile, Mo= molybdenite. Mineral abbreviation after [9].

## Elemental Distribution

The elemental distribution of host rock samples (RR.02.3 and RR09) is predominated by Si, Al, Fe, and K (Figure 5). These elements usually occur in silicate minerals such as K-feldspar, mica, and clays. These elements form a clay mineral that dominates the host rock sample in the form of wonesite, illite, kaolinite, montmorillonite, and chlorite. Other minerals composed of these elements are muscovite, oligoclase, albite, biotite, staurolite, and cordierite.

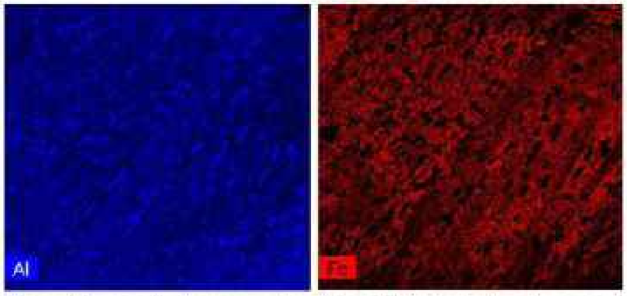

Figure 5. The distribution of dominant elements such as Al and Fe in the host rock sample indicates K-feldspar, mica, and clays distribution.

Uranium and REE are mainly found in the tourmaline and monazite ore samples. Si, Al, Fe, and Mg dominate the major element of tourmaline ore. These elements are found in tourmaline and wonesite minerals that are dominant in the sample. Uranium distribution in tourmaline ore concentrated along the veinlet associated with the Y element. The REE distribution can be divided into two groups, the Ce-Nd and Y groups. The Ce-Nd elements are closely associated and distributed randomly in the sample. On the other hand, Y is concentrated along the veinlet and at the edge of the tourmaline ore (Figure 6). The U-Y assemblages are incorporated in brannerite minerals, whereas Ce-Nd elements are incorporated in monazite, and Y s found in xenotime.

The elemental distributions in sample RR10, as monazite ore samples (Figure 7), are composed of Ce, La, P, and Nd, representing the monazite mineral. Uranium is distributed along the crack of the sample in the form of brannerite, uranophane, and swamboite

*p*-ISSN 0854-1418
*e*-ISSN 2503-426X

minerals. The cracks are filled with elements such as Fe, Si, Cu, and Mo. The Fe is incorporated either in almandine or chlorite; Si represents quartz, Cu represents the occurrence of native copper, and Mo represents molybdenite. REE in the monazite ore sample includes Ce, La, Nd, Sm, Gd, and Y. The last element is the primary element found in xenotime. Furthermore, Gd occurs in trace amount and mainly form loparite mineral, and uranium distribution in monazite ore is associated with the Y element in several veins or cracks. But the other REE elements, such as Ce, La, Nd, Sm, and Gd are the dominant element across the samples, indicating that the monazite ore is formed before the uranium mineralization.

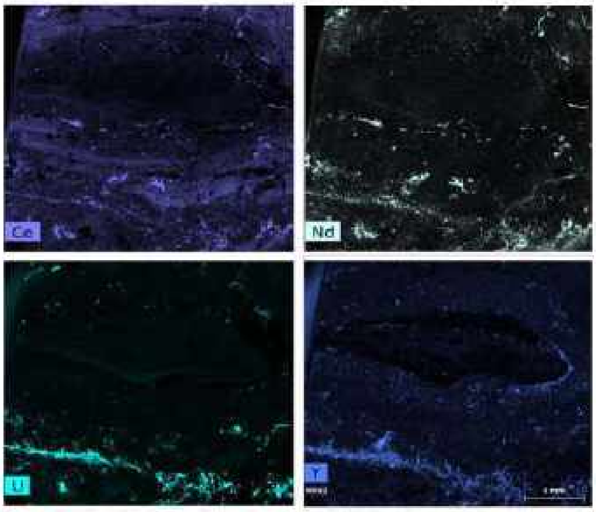

Figure 6. Distribution of uranium and REE in a tourmaline ore sample.

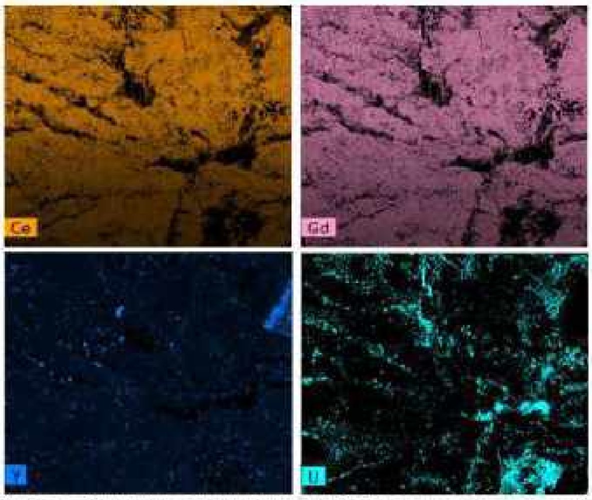

Figure 7. Distribution of uranium and REE in a monazite ore sample.

## Geochemistry

$SiO_2$ appears as the major element in the soil and host rock samples (ranges from 46.23 to 64.74%), much higher than the constituent in the monazite ore (1.46–16.73%). Subsequent major oxide compositions are $Fe_2O_3$, $Al_2O_3$, and $K_2O$ (Table 1). The silicate minerals dominate the soil and host rock and have undergone a weathering process, forming clays. In contrast, major oxides, such as CaO, MgO, MnO, $Cr_2O_3$, and $P_2O_5$, are relatively higher in monazite ore than in the soil or host rock sample. The presence of ore minerals such as monazite, apatite, and tourmaline cause the high concentration of these elements in monazite ore.

Table 2. Mayor oxide composition (wt.%) of soil, host rock, and monazite ore from the Rirang Sector.

| Element | Soil | | | | | | Host Rock | Monazite Ore | | |
|---|---|---|---|---|---|---|---|---|---|---|
| | RHS03 | RHS05 | RHS07 | RHS09 | RHS11 | RHS15 | RR09 | RR07 | RR13 | RR18 |
| $SiO_2$ | 49.29 | 60.21 | 64.74 | 49.77 | 46.23 | 50.06 | 61.93 | 7.67 | 16.73 | 1.46 |
| $Fe_2O_3$ | 9.31 | 7.10 | 12.17 | 8.27 | 13.65 | 12.81 | 7.14 | 2.19 | 3.03 | 1.13 |
| $Al_2O_3$ | 27.76 | 21.68 | 15.42 | 29.62 | 27.23 | 25.27 | 20.45 | 5.83 | 12.98 | 1.31 |
| CaO | <0.01 | <0.01 | <0.01 | <0.01 | <0.01 | <0.01 | 0.56 | 3.77 | 0.29 | 0.06 |
| MgO | 0.25 | 0.25 | 0.17 | 0.43 | 0.28 | 0.17 | 1.28 | 0.52 | 1.18 | 0.78 |
| MnO | <0.01 | <0.01 | 0.01 | 0.01 | 0.01 | 0.01 | 0.06 | 0.20 | 0.16 | 0.25 |
| $Cr_2O_3$ | 0.01 | 0.03 | 0.05 | 0.14 | 0.02 | 0.01 | 0.02 | 1.35 | 1.30 | 1.68 |
| $Na_2O$ | 1.28 | 1.05 | 0.74 | 2.25 | 1.07 | 1.31 | 1.74 | 1.90 | 1.63 | 1.38 |
| $K_2O$ | 4.39 | 1.75 | 0.51 | 6.09 | 2.67 | 3.44 | 2.65 | 2.71 | 2.55 | 0.53 |
| $TiO_2$ | 1.22 | 1.03 | 0.95 | 1.36 | 1.22 | 1.34 | 0.90 | 0.48 | 1.50 | 1.16 |
| $P_2O_5$ | 0.13 | 0.12 | 0.30 | 0.05 | 0.08 | 0.09 | 0.29 | 16.11 | 10.72 | 17.49 |
| LOI % | 8.42 | 8.38 | 7.21 | 7.35 | 10.31 | 7.67 | 4.45 | 2.55 | 3.32 | 0.87 |

The highest uranium concentration is found in monazite ore sample RR07, reaching 28,440 ppm, followed by other monazite ore RR18 (3,230 ppm), and RR13 (1,110 ppm). In the host rock sample, the uranium concentration reaches 391.96 ppm. In the soil sample, the uranium concentrations vary between 38.72–241.76 ppm (

Table 3), indicating that the uranium element has leached out during weathering and is concentrated mainly in the ore body of monazite and tourmaline ores. The total REE (TREE) concentration in monazite ore is about 85,320–13,8488 ppm. REE in monazite ore is dominantly composed of light REE (LREE), with concentrations ranging from 81,813 to 133,772 ppm. Meanwhile, heavy REE (HREE) concentration ranges from 1,472 to 2,532 ppm (Table 4).

The variation diagram of uranium compared to several major oxides and trace elements (Figure 8) shows that uranium has a positive correlation with $Na_2O$ and $P_2O_5$, indicating that uranium-bearing minerals are chemically composed of elements such as brannerite, uranophane, swamboite, loparite, and monazite. The positive correlation between uranium and $P_2O_5$ also indicates that apatite and xenotime form co-genetically during uranium mineralization[10]. On the contrary, the negative correlation between uranium and $Al_2O_3$ and $Fe_2O_3$ indicates that uranium is not associated with silicate and ferrous minerals such as clays and ferromagnesian minerals.

Table 3. Trace elements composition (ppm) of soil, host rock, and monazite ore from the Rirang Sector.

| Element | Soil | | | | | | Host Rock | Monazite Ore | | |
|---|---|---|---|---|---|---|---|---|---|---|
| | RHS03 | RHS05 | RHS07 | RHS09 | RHS11 | RHS15 | RR09 | RR07 | RR13 | RR18 |
| Li | 15.9 | 12.0 | 5.0 | 16.0 | 18.7 | 17.9 | 47.5 | 3.4 | 15.8 | 2.9 |
| Be | 1.9 | 1.1 | 1.0 | 2.0 | 2.1 | 2.4 | 2.6 | 0.5 | 1.2 | 0.4 |
| V | 184.6 | 164.2 | 240.9 | 187.1 | 218.7 | 190.5 | 134.3 | 312.8 | 199.5 | 82.3 |
| Co | 8.4 | 8.7 | 9.2 | 6.0 | 8.7 | 8.9 | 37.6 | 2.6 | 4.8 | 1.2 |
| Ni | 74.0 | 59.2 | 154.8 | 48.8 | 90.4 | 126.0 | 75.1 | 1.5 | 6.5 | <0.001 |
| Cu | 40.5 | 34.5 | 78.5 | 29.3 | 35.2 | 48.5 | 34.8 | 3.4 | 112.1 | 24.9 |
| Zn | 11.2 | 9.6 | 15.8 | 12.1 | 10.3 | 4.2 | 56.9 | 5.2 | 4.5 | 0.2 |
| Ga | 38.1 | 30.9 | 35.0 | 36.2 | 35.2 | 38.9 | 58.6 | 879.7 | 1,087.7 | 1,582.4 |
| As | 16.5 | 19.8 | 15.0 | 14.3 | 20.8 | 15.0 | 27.1 | 189.7 | 312.8 | 516.9 |
| Sc | 3.0 | 1.7 | 5.5 | 0.5 | 1.0 | 1.4 | 14.0 | 243.1 | 322.3 | 456.1 |
| Rb | 209.7 | 86.1 | 23.5 | 248.9 | 177.3 | 232.6 | 169.1 | 9.9 | 82.0 | 1.3 |
| Sr | 21.3 | 19.2 | 35.3 | 13.0 | 33.3 | 32.4 | 105.6 | 50.8 | 142.4 | 26.3 |
| Zr | 88.0 | 71.3 | 50.8 | 77.1 | 70.8 | 83.3 | 57.3 | 2.8 | 160.3 | 38.2 |
| Nb | 10.7 | 5.5 | 11.7 | 15.5 | 5.5 | 4.0 | 5.5 | 24.2 | 66.7 | 60.4 |
| Mo | 2,540.0 | 149.3 | 44.1 | 135.1 | 209.9 | 18.4 | 95.6 | 4,740.0 | 283.7 | 592.8 |
| Ag | 0.1 | 0.1 | 0.1 | 0.2 | 0.1 | 0.2 | 0.1 | 0.2 | 0.3 | 0.1 |
| Cd | 4.6 | 0.5 | 0.3 | 0.5 | 0.6 | 0.3 | 0.4 | 1.0 | 0.9 | 1.0 |
| [illegible] | 1.7 | 3.0 | 4.1 | 1.6 | 0.9 | 0.4 | 6.6 | 2.0 | 1.7 | <0.001 |
| Sb | 0.2 | 0.3 | 0.4 | 0.2 | 0.5 | 0.3 | 0.5 | 0.7 | 0.4 | 0.1 |
| Te | 0.2 | 0.2 | 0.2 | 0.1 | 0.1 | 0.1 | 0.1 | 0.4 | 0.4 | 0.2 |
| Cs | 3.8 | 2.8 | 1.4 | 3.9 | 5.7 | 6.4 | 6.5 | 0.5 | 0.9 | 0.2 |
| Ba | 481.8 | 250.2 | 77.2 | 568.4 | 281.1 | 372.6 | 316.6 | 53.2 | 575.4 | 17.9 |
| Hf | 2.5 | 2.2 | 1.9 | 2.4 | 1.9 | 2.5 | 2.0 | 11.8 | 14.4 | 18.4 |
| Ta | 0.9 | 0.7 | 1.1 | 1.3 | 0.5 | 0.5 | 0.7 | 2.1 | 2.9 | 3.0 |
| W | 4.7 | 3.4 | 6.5 | 5.5 | 2.1 | 1.3 | 3.4 | 19.7 | 39.0 | 13.8 |
| Pb | 59.7 | 25.2 | 115.2 | 27.6 | 6.7 | 6.9 | 88.2 | 3,840 | 1,260 | 1,550 |
| Bi | 0.3 | 0.4 | 0.5 | 0.2 | 0.2 | 0.2 | 0.4 | 0.4 | 0.6 | 0.2 |
| Th | 22.2 | 42.3 | 33.3 | 20.8 | 20.0 | 27.6 | 17.1 | 20.3 | 24.6 | 36.9 |
| U | 184.2 | 38.7 | 241.8 | 107.5 | 84.4 | 91.4 | 392.0 | 28,440.0 | 1,110.0 | 3,230.0 |

Table 4. REE composition (ppm) of soil, host rock, and monazite ore from the Rirang Sector.

| Element | Soil | | | | | | Host Rock | Monazite Ore | | |
|---|---|---|---|---|---|---|---|---|---|---|
| | RHS03 | RHS05 | RHS07 | RHS09 | RHS11 | RHS15 | RR09 | RR07 | RR13 | RR18 |
| La | 192.1 | 119.3 | 381.8 | 30.2 | 44.3 | 102.9 | 840.2 | 18,420 | 24,710 | 34,960 |
| Ce | 401 | 254.5 | 593.4 | 65.8 | 69.5 | 131.7 | 1,630 | 39,220 | 46,400 | > 50000 |
| Pr | 45.5 | 27.1 | 89.3 | 6.1 | 9.9 | 20.6 | 194.9 | 4,560 | 5,130 | 8,730 |
| Nd | 156.3 | 84.9 | 286.7 | 18.8 | 28.8 | 54.8 | 651.1 | 15,170 | 16,290 | 31,360 |
| Sm | 27.5 | 13.7 | 46.8 | 3.5 | 4.8 | 8.1 | 127.6 | 2,960 | 3,080 | 5,860 |
| Eu | 2.8 | 1.4 | 4.2 | 1 | 0.9 | 1.1 | 6.5 | 123.6 | 134.9 | 182 |
| Gd | 12.8 | 6.8 | 19.7 | 1.8 | 2.1 | 3.6 | 55.9 | 1,360.00 | 1,520.00 | 2,680.00 |
| Tb | 1.6 | 0.8 | 2.5 | 0.2 | 0.3 | 0.4 | 7.4 | 180.7 | 182.9 | 324.2 |
| Dy | 9.1 | 4.3 | 16.6 | 1.6 | 2.1 | 2.6 | 41.4 | 1,090.00 | 952.4 | 1,620.00 |
| Ho | 1.1 | 0.6 | 2.2 | 0.2 | 0.3 | 0.3 | 4.8 | 136.6 | 104.1 | 176.4 |
| Er | 2 | 1.1 | 3.9 | 0.6 | 0.7 | 0.8 | 8.3 | 239.4 | 149.4 | 257.9 |
| Tm | 0.3 | 0.1 | 0.4 | 0.1 | 0.1 | 0.1 | 0.9 | 27.4 | 13.9 | 24.8 |
| Yb | 1.6 | 1 | 2.3 | 0.7 | 0.9 | 0.9 | 4.8 | 140.9 | 57.3 | 106.3 |
| Lu | 0.2 | 0.1 | 0.3 | 0.1 | 0.1 | 0.1 | 0.7 | 19.7 | 12.1 | 22.8 |
| Sc | 28.4 | 23.8 | 30.3 | 35 | 36.4 | 32.6 | 22.3 | 32.4 | 20.5 | 4.7 |
| Y | 10.4 | 8.5 | 22.9 | 3.6 | 4.8 | 4.9 | 76.4 | 1,640.00 | 1,130.00 | 2,180.00 |
| TREE | 892.8 | 548.2 | 1,503.30 | 169.2 | 206 | 365.5 | 3,673.30 | 85,320.80 | 99,887.40 | 138,488.90 |
| $(La/Yb)_N$ | 79 | 84.1 | 113.7 | 30.3 | 34.9 | 80.3 | 118.7 | 88.3 | 291.3 | 222.3 |
| $(La/Sm)_N$ | 4.4 | 5.5 | 5.1 | 5.4 | 5.8 | 8 | 4.1 | 3.9 | 5 | 3.8 |
| $(Gd/Yb)_N$ | 6.3 | 5.8 | 7 | 2.2 | 2 | 3.4 | 9.5 | 7.8 | 21.5 | 20.4 |

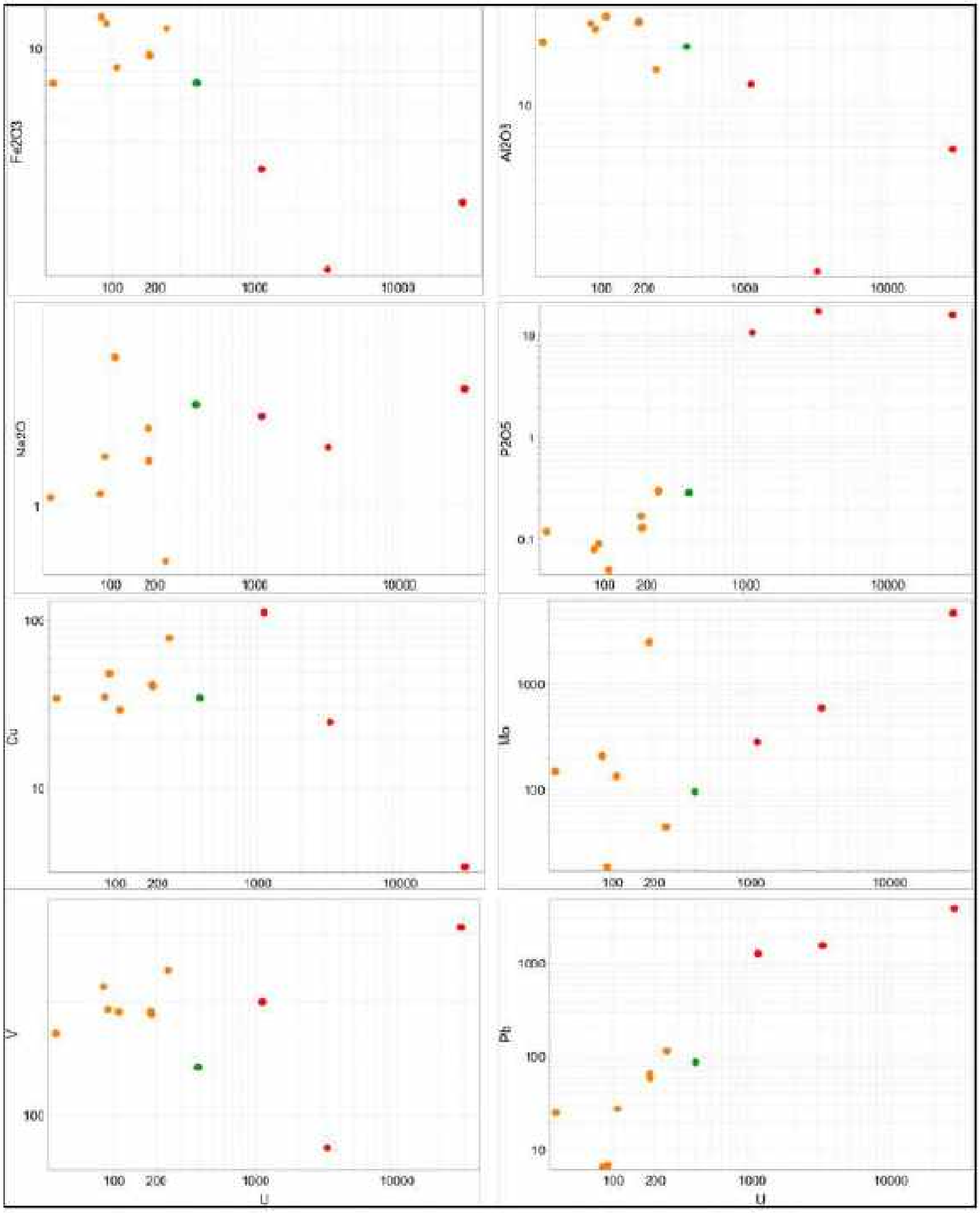

Figure 8. Variation diagram of uranium versus several major oxides and trace elements.

Compared to other elements, uranium exhibits a relatively strong positive correlation with marker elements of hydrothermal alteration products, including Cu, Mo, V, and Pb. Positive correlation suggests that these elements are enriched during the uranium mineralization process. U-Cu and U-Mo correlation shows relatively higher enrichment in the soil sample than other elements. Mo and Cu are believed to be adsorbed to the clay

*p*-ISSN 0854-1418
*e*-ISSN 2503-426X

mineral during the weathering process. They are derived from the leaching process of host minerals, such as biotite, magnetite, hornblende K-feldspar, plagioclase, and ilmenite[11].

The variation diagram of TREE and several major oxides, uranium, and trace element (Figure 9) shows positive correlations with $Na_2O$ and $P_2O_5$, indicating that REE are mainly incorporated into phosphate or sodium oxide minerals as the REE-bearing minerals such as monazite, xenotime, apatite, and loparite. Mn oxide plays an important role in the distribution of REE because Mn oxides can bind REE through several processes, such as coprecipitation, adsorption, and ion exchange[12]. The $Na_2O$ and REE tend to become enriched in post-magmatic hydrothermal fluids. As a result, these elements are often closely associated with each other. On the other hand, TREE shows a negative correlation to $Al_2O_3$ and $Fe_2O_3$, indicating that REE is not enriched in clay-rich rocks or highly weathered soil. TREE shows a positive correlation compared to uranium and other trace elements such as Cu, V, and Pb. The data indicate that TREE and uranium are co-genetically concentrated during hydrothermal alteration.

The C1 Chondrite normalization[13] in the trace element diagram (Figure 10a) shows that the HFSE and LILE exhibited a greater depletion pattern than the Upper Continental Crust (UCC)[14] and the Post Archean Australian Shale (PAAS) [15]. On the other hand, uranium and REE show enrichment patterns, except for Eu, which shows depletion. The Eu depletion, followed by Sr and K depletion, indicates the weathering process of plagioclase[16]. In addition, the Eu depletion also indicates plagioclase fractionation in the magma source[12], [14].

The multi-element diagram of the REE-C1 chondrite (Figure 10b) shows an LREE enrichment and an HREE depletion pattern. These patterns indicate two alteration types during the uranium mineralization process, K-feldspar alteration and silicification[17], [18]. These patterns are also similar to the typical monazite that probably act as the main source of REE analyzed in the sample. The REE pattern in the soil sample shows similarity to the ore and host rock sample but has a lower value. The lower value indicates an early leaching phase of weathering process[19], [20].

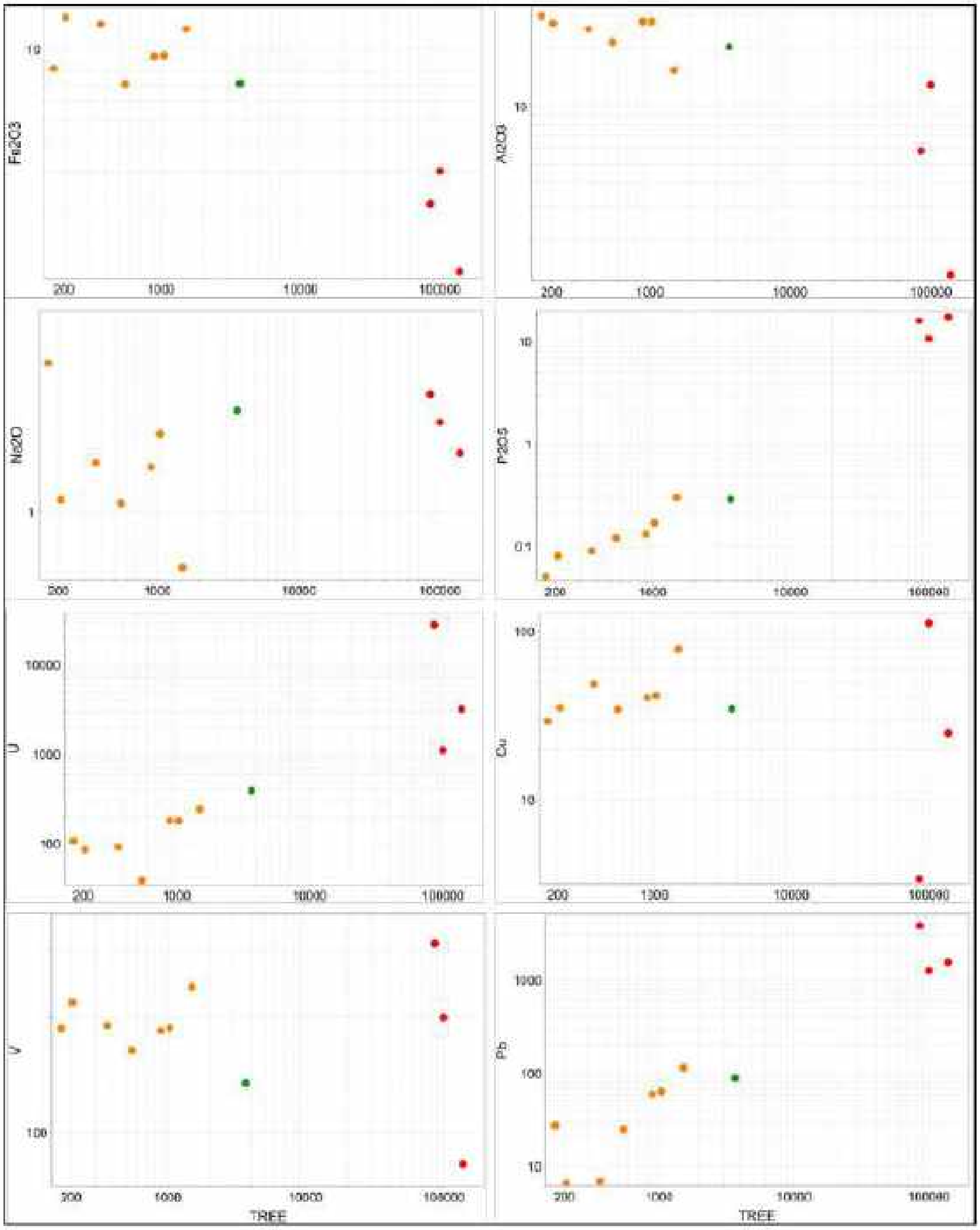

Figure 9. Variation diagram of TREE versus several major oxides and trace elements.

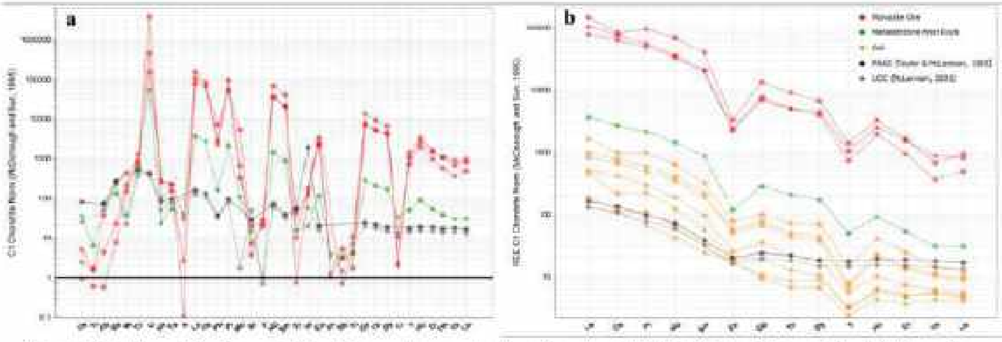

Figure 10. The multi-element plot of monazite ore, host rock, and soil in the Rirang Sector, West Kalimantan. a) Monazite ore and metasiltstone host rock show a depletion pattern in HSFE and LILE and enrichment in uranium and REE. b) Monazite ore, host rock, and soil show enrichment patterns in LREE and depletion patterns in HREE.

## DISCUSSION

The host rock for uranium and REE mineralization in the Rirang Sector are metamorphic rocks, including metapelite and metasiltstone. The metamorphic rocks were characterized by slaty to phyllitic foliation and spotted shale textures. The spotted shale texture is a result of clay minerals from weathered andalusite minerals, like wonesite and kaolinite. The occurrences of almandine, cordierite, and staurolite minerals indicate the regional metamorphism process. Paragenesis consisting of muscovite, almandine, and andalusite minerals indicates that the area's metamorphism facies were greenschist facies.

The rocks' REE pattern and Eu anomaly indicate the source rock characteristics[15]. A high LREE/HREE ratio and negative Eu anomaly are commonly found in granitic rocks[21]–[23]. The C1 Chondrite normalized REE plot shows a fractionated REE pattern ($(La/Yb)_N$ = 88.31–291.34, mean = 180.15), characterized by highly fractionated LREE ($(La/Sm)_N$ = 3.75–5.05, mean = 4.21) and HREE ($(Gd/Yb)_N$ = 7.82–21.49, mean = 14.8). In addition, REE pattern shows negative Eu anomaly, positive Ce anomaly, and enriched LREE/HREE ratio. This suggests that meta-siltstone and monazite ore are derived from felsic source rocks [24]. The granite intrusions north of the Rirang Sector (Figure 1) are strongly expected as a source of uranium and REE-bearing fluid. Uranium, REE, and several trace elements are commonly soluble in Na-rich rather than K-rich fluid. The occurrences of oligoclase and albite in the tourmaline and monazite ore characterize the Na-rich fluids. Moreover, Na-rich calc-silicate minerals such as hornblende associated with albite and oligoclase indicated the occurrence of sodic alteration [25]. On the other hand, the mineralization of brannerite, uranophane, and swamboite also indicated that the Na-metasomatism process occurred at medium temperatures [26]–[29]. The source of this metasomatism process is due to granitic intrusion in the north of the Rirang Sector and regionally correlated as Sukadana Granite.

The Rirang Sector is characterized by various mineralization and alteration processes that form several uranium and REE-bearing minerals, such as brannerite, uranophane, swamboite, monazite, xenotime, apatite, and loparite. Monazite, xenotime, apatite, and loparite are dominant LREE host minerals among these minerals. The high LREE/HREE ratio and negative Eu anomaly observed in the monazite ore indicated that these minerals originated from the felsic igneous source rocks.

In the samples studied, brannerite is the primary uranium-bearing mineral. This mineral cross-cuts the tourmaline and monazite ore, indicating that brannerite is formed in a later phase than both ores. Subsequently, brannerite is associated with pyrite, molybdenite, ilmenite, magnetite, rutile, and hematite, indicating the occurrence of the hydrothermal process during mineralization. Swamboite and uranophane are the later uranium mineral that formed resulting from the groundwater oxidation of brannerite [30].

The soil in the Rirang Sector, produced through weathering processes, exhibits a similar REE pattern to the host rocks and monazite ore. This similar pattern indicates an early phase leaching process of the monazite ore and host rock due to weathering [19], [20]. In some cases, weathering process can enrich the REE content in the soil [17], [28], [29], [31], with the main factor controlling the enrichment being clay minerals such as smectite, illite, kaolinite, and halloysite that act as adsorption agent of REE ions [19], [20], [32], [33]. In the Rirang sector, the clay mineral products are wonesite, illite, and kaolinite. Hence, the REE ions leach into the groundwater.

## CONCLUSION

The Rirang Sector in West Kalimantan contains metapelite and metasiltstone that contain uranium and rare earth element (REE) mineralization. The dominant clay minerals in these rocks are derived from volcanic sources, and the alteration minerals are a product of hydrothermal alteration. Tourmaline and monazite ores are associated with uranium and REE mineralization. On the other hand, REE mineralization occurs in the form of monazite, xenotime, and loparite. The enrichment of uranium, REE, and other trace elements are believed to be due to their association with the Na-rich fluid of felsic intrusion. The north of the Rirang Sector's felsic intrusions correlates with the Sukadana Granite on the regional scale. The enrichment process of REE is apparently due to the fractional crystallization of felsic fluid forming monazite, xenotime, apatite, and loparite. Furthermore, uranium enrichment is related to hydrothermal alteration, forming brannerite, uranophane, and other alteration minerals such as molybdenite, pyrite, copper, rutile, ilmenite, and magnetite. The interaction of the uranium-bearing mineral and groundwater forms secondary uranium mineral swamboite. The weathering process does not enrich the uranium and REE content in the soil but tend to decrease due to the leaching process and the absence of clay minerals that capable of binding REE ions into the soil.

## ACKNOWLEDGMENT

The authors are grateful to the National Research and Innovation Agency for providing the funding and facility to conduct this investigation. We also thank the anonymous reviewers for their thorough reviews and helpful suggestions.

## REFERENCES

[1] Ngaderin, A. Sumaryanto, H. Syaeful, and I. G. Sukadana, "Geologi dan Mineralisasi Uranium di Daerah Kalan, Kabupaten Melawi, Kalimantan Barat," in *Seminar Nasional Kebumian XII*, Yogyakarta: Fakultas Teknologi Mineral, Universitas Pembangunan Nasional "Veteran" Yogyakarta, 2017, pp. 108–114.

[2] Ngadenin, I. G. Sukadana, and R. Fauzi, "Preliminary overview of the prospects for rare earth elements in Kalan , West Kalimantan , Indonesia Preliminary Overview of The Prospects for Rare Indonesia," in *AIP Conference Proceedings*, 2022, pp. 1–11.

[3] Suharji, Ngadenin, Wagiyanto, and Sumarno, "Peningkatan Kwalitas Estimasi Cadangan

Uranium dan Unsur Tanah Jarang Sebagai Asosiasinya di Sektor Rirang Hulu, Kalimantan Barat," *Pros. Semin. IPTEK Nukl. dan Pengelolaan Sumber Daya Tambang*, pp. 51–65, 2002.

[4] S. Tjokrokardono, "Studi Provinsi Uranium Kalimantan; Kajian Mineralisasi Uranium Pada Batuan Metamorf Dan Granit Di Pegunungan Schwaner," *Seminar IPTEK Nuklir dan Pengelolaan Sumber Daya Tambang*, 2002.

[5] S. Tjokrokardono, L. Subiantoro, and M. Widodo, "Sintesis Geologi dan Mineralisasi Uranium Kalan dan Sekitarnya, Kalimantan Barat," Jakarta, 2006.

[6] B. Soetopo, R. Witjahyati, and Y. Wusana, "Sintesa Geologi dan Pemineralan Uranium Sektor Rabau Hulu, Kalan, Kalimantan Barat," *Semin. Geol. Nukl. dan Sumberd. Tambang Tahun 2004*, pp. 85–99, 2004.

[7] D. Savira, M. A. Gunawan, W. A. Draniswari, I. G. Sukadana, and F. Sihombing, "μxRF Application for Uranium Exploration (Case Study: Mamuju Deposit, Indonesia)," *IOP Conf. Ser. Earth Environ. Sci.*, vol. 830, no. 1, 2021, doi: 10.1088/1755-1315/830/1/012076.

[8] I. G. Sukadana, I. W. Warmada, F. Pratiwi, A. Harijoko, T. B. Adimedha, and A. W. Yogatama, "Elemental Mapping for Characterizing of Thorium and Rare Earth Elements (REE) Bearing Minerals Using μXRF," *Atom Indones.*, vol. 48, no. 2, pp. 87–98, 2022, doi: 10.17146/aij.2022.1215.

[9] L. N. Warr, "IMA–CNMNC approved mineral symbols," *Mineral. Mag.*, vol. 85, no. 3, pp. 291–320, 2021, doi: 10.1180/mgm.2021.43.

[10] P. Alexandre, "Mineralogy and geochemistry of the sodium metasomatism-related uranium occurrence of Aricheng South, Guyana," *Miner. Depos.*, vol. 45, no. 4, pp. 351–367, 2010, doi: 10.1007/s00126-010-0278-7.

[11] J. A. Plant, P. R. Simpson, B. Smith, and B. F. Windley, "Uranium ore deposits-products of the radioactive earth," *Uranium Mineral. Geochemistry, Environ.*, no. September, pp. 255–319, 2019, doi: 10.1515/9781501509193-011.

[12] X. P. Yan, R. Kerrich, and M. J. Hendry, "Sequential leachates of multiple grain size fractions from a clay-rich till, Saskatchewan, Canada: Implications for controls on the rare earth element geochemistry of porewaters in an aquitard," *Chem. Geol.*, vol. 158, no. 1–2, pp. 53–79, 1999, doi: 10.1016/S0009-2541(99)00011-X.

[13] W. F. McDonough and S. s. Sun, "The composition of the Earth," *Chem. Geol.*, vol. 120, no. 3–4, pp. 223–253, 1995, doi: 10.1016/0009-2541(94)00140-4.

[14] S. M. McLennan, "Relationships between the trace element composition of sedimentary rocks and upper continental crust," *Geochemistry, Geophys. Geosystems*, vol. 2, 2001, doi: 10.1038/scientificamerican0983-130.

[15] S. R. Taylor and S. M. McLennan, *The continental crust: Its composition and evolution*. 1985.

[16] C. Wang, L. Zhang, Y. Dai, and C. Lan, "Geochronological and geochemical constraints on the origin of clastic meta-sedimentary rocks associated with the Yuanjiacun BIF from the Lüliang Complex, North China," *Lithos*, vol. 212–215, pp. 231–246, 2015, doi: 10.1016/j.lithos.2014.11.015.

[17] Z. Bao and Z. Zhao, "Rare-earth element mobility during ore-forming hydrothermal alteration: A case study of Dongping gold deposit, Hebei Province, China," *Chinese J. Geochemistry*, vol. 22, no. 1, pp. 45–57, 2003, doi: 10.1007/bf02831545.

[18] S. Akhtar, X. Yang, and F. Pirajno, "Sandstone type uranium deposits in the Ordos Basin, Northwest China: A case study and an overview," *J. Asian Earth Sci.*, vol. 146, no. September 2016, pp. 367–382, 2017, doi: 10.1016/j.jseaes.2017.05.028.

[19] Y. Kanazawa and M. Kamitani, "Rare earth minerals and resources in the world," in *Journal of Alloys and Compounds*, Feb. 2006, pp. 1339–1343. doi: 10.1016/j.jallcom.2005.04.033.

[20] A. Berger, E. Janots, E. Gnos, R. Frei, and F. Bernier, "Rare earth element mineralogy and geochemistry in a laterite profile from Madagascar," *Appl. Geochemistry*, vol. 41, pp. 218–228, 2014, doi: 10.1016/j.apgeochem.2013.12.013.

[21] G. W. A. Nyakairu and C. Koeberl, "Mineralogical and chemical composition and distribution of rare earth elements in clay-rich sediments from central Uganda," *Geochem. J.*, vol. 35, no. 1, pp. 13–28, 2001, doi: 10.2343/geochemj.35.13.

[22] B. K. Das, A. S. AL-Mikhlafi, and P. Kaur, "Geochemistry of Mansar Lake sediments, Jammu, India: Implication for source-area weathering, provenance, and tectonic setting," *J. Asian Earth Sci.*, vol. 26, no. 6, pp. 649–668, 2006, doi: 10.1016/j.jseaes.2005.01.005.

[23] R. Kritsananuwat, S. K. Sahoo, M. Fukushi, and S. Chanyotha, "Distribution of rare earth elements, thorium and uranium in Gulf of Thailand's sediments," *Environ. Earth Sci.*, vol. 73, no. 7, pp. 3361–3374, 2015, doi: 10.1007/s12665-014-3624-8.

[24] D. Bakkiaraj, R. Nagendra, R. Nagarajan, and J. S. Armstrong-Altrin, "Geochemistry of sandstones from the upper Cretaceous sillakkudi Formation, Cauvery basin, Southern India: Implication for provenance," *J. Geol. Soc. India*, vol. 76, no. 5, pp. 453–467, 2010, doi: 10.1007/s12594-010-0128-3.

[25] R. G. Skirrow *et al.*, *Uranium Mineral Systems : Processes , exploration criteria and a new deposit framework*. Geosciences Australia Record 2009/20, 2009.

[26] A. D. Mckay and Y. Miezitis, "Australia's uranium resources, geology and development of deposits.," 2001. doi: 10.1159/000335161.

[27] P. A. Polito and T. K. Kyser, "The Valhalla Uranium Deposit, Qeensland, Australia," *ASEG Ext. Abstr.*, vol. 2006, no. 1, pp. 1–4, 2006, doi: 10.1071/aseg2006ab140.

[28] M. Cuney and K. Kyser, "Recent and not-so-recent developments in uranium deposits and implications for exploration," *Short Course Ser. Vol. 39*, vol. 39, no. January 2009, p. 259, 2008.

[29] M. Cuney, A. Emetz, J. Mercadier, V. Mykchaylov, V. Shunko, and A. Yuslenko, "Uranium deposits associated with Na-metasomatism from central Ukraine: A review of some of the major deposits and genetic constraints," *Ore Geol. Rev.*, vol. 44, pp. 82–106, 2012, doi: 10.1016/j.oregeorev.2011.09.007.

[30] P. Bruneton and M. Cuney, *Geology of uranium deposits*, no. 1956. Elsevier Ltd, 2016. doi: 10.1016/B978-0-08-100307-7.00002-8.

[31] M. Bau, "Rare-earth element mobility during hydrothermal and metamorphic fluid-rock interaction and the significance of the oxidation state of europium," *Chem. Geol.*, vol. 93, no. 3–4, pp. 219–230, 1991, doi: 10.1016/0009-2541(91)90115-8.

[32] G. Estrade, E. Marquis, M. Smith, K. Goodenough, and P. Nason, "REE concentration processes in ion adsorption deposits: Evidence from the Ambohimirahavavy alkaline complex in Madagascar," *Ore Geol. Rev.*, vol. 112, no. March, p. 103027, 2019, doi: 10.1016/j.oregeorev.2019.103027.

[33] D. Wang *et al.*, "Exploration and research progress on ion-adsorption type REE deposit in South China," *China Geol.*, vol. 1, no. 3, pp. 414–423, 2018, doi: 10.31035/cg2018022.

# Distribution and Characteristics of Rare Earth Elements in Uranium-Ore Deposits from Rirang Area, West Kalimantan Province, Indonesia

ORIGINALITY REPORT

| 10% | 6% | 7% | 1% |
|---|---|---|---|
| SIMILARITY INDEX | INTERNET SOURCES | PUBLICATIONS | STUDENT PAPERS |

PRIMARY SOURCES

| | | |
|---|---|---|
| 1 | eprints.upnyk.ac.id<br>Internet Source | 1% |
| 2 | Xiaolin Ou, Zhibiao Chen, Xiuling Chen, Xiaofei Li et al. "Redistribution and chemical speciation of rare earth elements in an ion–adsorption rare earth tailing, Southern China", Science of The Total Environment, 2022<br>Publication | 1% |
| 3 | munispace.muni.cz<br>Internet Source | 1% |
| 4 | Ngadenin, I. Gde Sukadana, Rachman Fauzi. "Preliminary overview of the prospects for rare earth elements in Kalan, West Kalimantan, Indonesia", AIP Publishing, 2022<br>Publication | 1% |
| 5 | digital.library.adelaide.edu.au<br>Internet Source | 1% |

| | | |
|---|---|---|
| 6 | eul.army.mil<br>Internet Source | <1 % |
| 7 | Abdou Dodo Bohari, Moussa Harouna, Ali Mosaad. "Geochemistry of Sandstone Type Uranium Deposit in Tarat Formation from Tim-Mersoi Basin in Northern Niger (West Africa): Implication on Provenance, Paleo-Redox and Tectonic Setting", Journal of Geoscience and Environment Protection, 2018<br>Publication | <1 % |
| 8 | doaj.org<br>Internet Source | <1 % |
| 9 | link.springer.com<br>Internet Source | <1 % |
| 10 | D. Bakkiaraj, R. Nagendra, R. Nagarajan, John S. Armstrong-Altrin. "Geochemistry of sandstones from the Upper Cretaceous Sillakkudi Formation, Cauvery Basin, southern India: Implication for provenance", Journal of the Geological Society of India, 2011<br>Publication | <1 % |
| 11 | R A Farrenzo, R D Nugraheni, I G Sukadana, F D Indrastomo, T B Adimedha. "Characterization of Metapelite and Metasiltstone as Uranium-REE hosted rocks in Rirang Area, West Kalimantan", IOP | <1 % |

| | | |
|---|---|---|
| | Conference Series: Earth and Environmental Science, 2023<br>Publication | |
| 12 | R. Nagarajan, Priyadarsi D. Roy, M.P. Jonathan, Rufino Lozano, Franz L. Kessler, M.V. Prasanna. "Geochemistry of Neogene sedimentary rocks from Borneo Basin, East Malaysia: Paleo-weathering, provenance and tectonic setting", Geochemistry, 2014<br>Publication | <1 % |
| 13 | series.ump.edu.my<br>Internet Source | <1 % |
| 14 | hal.inria.fr<br>Internet Source | <1 % |
| 15 | www.fesb.hr<br>Internet Source | <1 % |
| 16 | jrisetgeotam.lipi.go.id<br>Internet Source | <1 % |
| 17 | D GASQUET, J LETERRIER, Z MRINI, P VIDAL. "Petrogenesis of the Hercynian Tichka plutonic complex (Western High Atlas, Morocco): Trace element and RbSr and SmNd isotopic constraints", Earth and Planetary Science Letters, 1992<br>Publication | <1 % |
| 18 | Gehan A. M. Aly. "Mineralogical and geochemical aspects of Miocene laterite, | <1 % |

| | | |
|---|---|---|
| | Sharm Lollia area, South Eastern Desert, Egypt", Arabian Journal of Geosciences, 2015<br>Publication | |
| 19 | Miruo Lin, Kelai Xi, Yingchang Cao, Keyu Liu, Rukai Zhu. "Periodic paleo-environment oscillation on multi-timescales in the Triassic and their significant implications for algal blooms: A case study on the lacustrine shales in Ordos Basin", Palaeogeography, Palaeoclimatology, Palaeoecology, 2022<br>Publication | <1 % |
| 20 | Windi Anarta Draniswari, Fadiah Pratiwi, Ngadenin Ngadenin, I Gde Sukadana et al. "Distribution and Mineralogical Characteristic of Raya Volcanics, West Kalimantan", EKSPLORIUM, 2021<br>Publication | <1 % |
| 21 | scholar.uwindsor.ca<br>Internet Source | <1 % |
| 22 | Armstrong-Altrin, John S., Ramasamy Nagarajan, Vysetti Balaram, and Olmedo Natalhy-Pineda. "Petrography and geochemistry of sands from the Chachalacas and Veracruz beach areas, western Gulf of Mexico, Mexico: Constraints on provenance and tectonic setting", Journal of South American Earth Sciences, 2015.<br>Publication | <1 % |

|  |  |  |
|---|---|---|
| 23 | Bao Zhiwei, Zhao Zhenhua. "Rare-earth element mobility during ore-forming hydrothermal alteration: A case study of Dongping gold deposit Hebei Province, China", Chinese Journal of Geochemistry, 2003<br>Publication | <1% |
| 24 | Dill, H.G.. "The ''chessboard'' classification scheme of mineral deposits: Mineralogy and geology from aluminum to zirconium", Earth Science Reviews, 201006<br>Publication | <1% |
| 25 | Ming Ma, Guojun Chen, Chao Li, Gongcheng Zhang, Chengfu Lv, Lianhua Xue, Huailei Shen, Zhao Zhao. "Petrography and geochemistry of Oligocene to Lower Miocene sandstones in the Baiyun Sag, Pearl River Mouth Basin, South China Sea: Provenance, source area weathering, and tectonic setting", Geological Journal, 2018<br>Publication | <1% |
| 26 | R. Nagarajan, J.S. Armstrong-Altrin, F.L. Kessler, J. Jong. "Petrological and Geochemical Constraints on Provenance, Paleoweathering, and Tectonic Setting of Clastic Sediments From the Neogene Lambir and Sibuti Formations, Northwest Borneo", Elsevier BV, 2017 | <1% |

Publication

27 Sahoo, Prafulla Kumar, Pedro Walfir Martins Souza-Filho, José Tasso Felix Guimarães, Marcio Sousa da Silva, Francisco Ribeiro Costa, Carmem-Lara de Oliveira Manes, Douglas Oti, Renato Oliveira Silva Júnior, and Roberto Dall'Agnol. "Use of multi-proxy approaches to determine the origin and depositional processes in modern lacustrine sediments: Carajás Plateau, Southeastern Amazon, Brazil", Applied Geochemistry, 2015. <1%

Publication

28 Sako, A.. "Rare earth and trace element geochemistry of termite mounds in central and northeastern Namibia: Mechanisms for micro-nutrient accumulation", Geoderma, 20091015 <1%

Publication

29 Vermeire, Marie-Liesse, Sophie Cornu, Zuzana Fekiacova, Marie Detienne, Bruno Delvaux, and Jean-Thomas Corn�lis. "Rare earth elements dynamics along pedogenesis in a chronosequence of podzolic soils", Chemical Geology, 2016. <1%

Publication

30 Wei Fu, Peng Luo, Zuoying Hu, Yangyang Feng, Lei Liu, Jingbao Yang, Meng Feng, Hongxia Yu, Yongzhang Zhou. "Enrichment of <1%

| | | |
|---|---|---|
| | ion-exchangeable rare earth elements by felsic volcanic rock weathering in South China: Genetic mechanism and formation preference", Ore Geology Reviews, 2019<br>Publication | |
| 31 | Zaid, Samir M.. "Provenance, diagenesis, tectonic setting and reservoir quality of the sandstones of the Kareem Formation, Gulf of Suez, Egypt", Journal of African Earth Sciences, 2013.<br>Publication | <1 % |
| 32 | aij.batan.go.id<br>Internet Source | <1 % |
| 33 | comptes-rendus.academie-sciences.fr<br>Internet Source | <1 % |
| 34 | theses.hal.science<br>Internet Source | <1 % |
| 35 | www.frontiersin.org<br>Internet Source | <1 % |
| 36 | www.journals.uchicago.edu<br>Internet Source | <1 % |

| | | | |
|---|---|---|---|
| Exclude quotes | On | Exclude matches | Off |
| Exclude bibliography | On | | |